DRAFT VERSION DECEMBER 8, 1999
Preprint typeset using LaTeX style emulateapj

THE LOW-MASS STELLAR CONTENT OF THE SCORPIUS-CENTAURUS OB ASSOCIATION [a]

[a]BASED ON OBSERVATIONS OBTAINED AT THE EUROPEAN SOUTHERN OBSERVATORY (ESO PROP. ID. 49.7-0065, 51.6-0002, 53.6-0016, 53.6-0017, 55.E-0934), AND ON OBSERVATIONS MADE WITH THE RÖNTGENSATELLIT (ROSAT), AND WITH THE NASA/ESA HUBBLE SPACE TELESCOPE, OBTAINED AT THE SPACE TELESCOPE SCIENCE INSTITUTE, WHICH IS OPERATED BY THE ASSOCIATION OF UNIVERSITIES FOR RESEARCH IN ASTRONOMY, INC., UNDER NASA CONTRACT NAS5-26555.

MICHAEL KUNKEL[2], WOLFGANG BRANDNER[3], HAROLD W. YORKE[4,2], HANS ZINNECKER[5], RALPH NEUHÄUSER[6], JÜRGEN H.M.M. SCHMITT[7], MICHEL MAYOR[8], STÉPHANE UDRY[8]

[2]Astronomisches Institut der Universität Würzburg, Am Hubland, D-97074 Würzburg, Germany; Michael.Kunkel@skf.com
[3]Institute for Astronomy, University of Hawaii, 2680 Woodlawn Dr., Honolulu, HI 96822, USA; brandner@ifa.hawaii.edu
[4]JPL, 4800 Oak Grove Drive, Mail Stop 169-506, Pasadena, CA 91109, USA; Harold.Yorke@jpl.nasa.gov
[5]Astrophysikalisches Institut Potsdam, An der Sternwarte 16, D-14482 Potsdam, Germany; hzinnecker@aip.de
[6] Max-Planck-Institut für extraterrestrische Physik, D-85740 Garching, Germany; rne@xray.mpe.mpg.de
[7] Sternwarte Universität Hamburg, Germany; jschmitt@hs.uni-hamburg.de
[8]Observatoire de Genève, CH-1290 Sauverny, Switzerland; Michel.Mayor@obs.unige.ch; Stephane.Udry@obs.unige.ch

Draft version December 8, 1999

ABSTRACT

Based on ROSAT observations and data obtained with ground-based telescopes, we have carried out an extensive study of the low-mass pre-main-sequence population in Upper Scorpius, the youngest subgroup of the Scorpius-Centaurus OB association. In this data paper we present the observations, and a preliminary analysis and interpretation of the results. Combined with data from a study of Upper Scorpius by another group a total of 118 X-ray active late-type stars with at least traces of lithium absorption in their spectra could be identified. An attempt to place the stars in an HR-diagram in order to derive masses and ages is problematic for two reasons: first, high-resolution imaging and spectroscopy reveal a high incidence binary and multiple systems. Deriving the evolutionary status for the unresolved systems from their position in an HR-diagram would lead to an overestimate of the mass and an underestimate of the age of the population of young, X-ray active, late-type stars in Upper Scorpius. Secondly, HIPPARCOS parallaxes for a small subset reveal a spread in distances by at least a factor of 2, which makes luminosity estimates uncertain by a factor of 4 when assuming a fixed distance for all the stars in the sample. We conclude that ages and masses for X-ray active late-type stars in Upper Scorpius cannot reliably be derived unless multiplicity and distance uncertainties are properly taken into account. An analysis of the spectral properties reveals that 7 stars in the sample can be classified as classical T Tauri stars (CTTS), 20 as weak-line T Tauri stars (WTTS), 49 as post-T Tauri stars (PTTS), and 42 stars remain unclassified. Furthermore, CTTS and WTTS tend to be associated with the dark clouds near ρ Oph and with B40, whereas PTTS are spread out over the entire area under study. The majority of low-mass stars in Upper Scorpius appears to be at least as old as the B-type stars. Star formation ceased after the formation of the high-mass stars. The sample of 49 genuine post-T Tauri stars will prove valuable for future studies of the timescales of disk evolution and planet formation around young solar-type stars.

Subject headings: open clusters and associations: individual (Sco OB2) — Galaxy: stellar content — stars: pre-main sequence — stars: late-type

1. INTRODUCTION

Scorpius-Centaurus (Sco OB2) at an average distance of 150 pc is the nearest OB-association. It is part of Gould's belt, a hyperstructure of star forming regions in the Solar neighborhood (e.g., Poeppel 1997). The high-mass stellar content of Sco OB2 was studied by de Geus, de Zeeuw, & Lub (1989) using Walraven photometry, and more recently by de Zeeuw et al. (1999), based on data obtained with the HIPPARCOS satellite. HIPPARCOS confirms the presence of 3 previously discovered spatially and kinematically distinct subgroups (see Blaauw 1991, and references therein). A total of 521 mostly early type stars were identified as likely members of the Scorpius-Centaurus association. According to de Geus et al. (1989), the three subgroups have ages ranging from 5 to 15 Myr. To the east and south of Upper Scorpius, the youngest subgroup of the OB association, are the dark clouds near ρ Ophiuchi and in Lupus, respectively. These dark clouds appear to be the only remnants of a once giant molecular cloud which gave birth to the Scorpius-Centaurus OB-association.

The main motivation for our study was to investigate to what extent OB associations form low-mass stars, whether the low-mass initial mass function (IMF) in OB associations is the same as the field IMF, and whether low- and

high-mass stars in an OB association are coeval and form at the same time. The first study of low-mass stars in Upper Scorpius based on X-ray observations with HEAO 2 ("EINSTEIN") was carried out by Walter et al. (1994), who identified 28 low-mass pre-main-sequence stars as likely members of Upper Scorpius. Walter et al. (1994) came to the surprising conclusion that the low-mass stars in Upper Scorpius (age 1-2 Myr) are significantly younger than the more massive early type stars of spectral type B and A (age 5-6 Myr). A more recent study by Preibisch & Zinnecker (1999) based on EINSTEIN and ROSAT observations, and covering a larger area, but with significant less sensitivity, however, came to a different conclusion. The 86 low-mass stars in their sample appear to be coeval to the 5 to 6 Myr old high-mass stars in Upper Scorpius.

In this data paper we present the ROSAT and ground-based follow-up observations, and a first analysis and interpretation of some of the findings. The limiting B-magnitude of our survey is $18\overset{m}{.}6$ with a median value of $13\overset{m}{.}9$ and is on average about 1 mag deeper than the survey by Preibisch et al. (1998).

2. OBSERVATIONS AND DATA ANALYSIS

2.1. *ROSAT Observations*

The Röntgensatellit (ROSAT, Trümper 1983) was launched in June 1990. During the first 7 months of its mission, the X-ray satellite carried out the ROSAT All Sky Survey (RASS) using its Position Sensitive Proportional Counter (PSPC). Because of the location of Scorpius-Centaurus close to the ecliptic plane and the South Atlantic Anomaly, effective exposure times of the RASS in the direction of Scorpius-Centaurus are only of the order of 500s to 600s. The present study concentrates on an area confined to the west by the older subgroup Upper Centaurus-Lupus, to the south by the Lupus T association, and to the northeast by ρ Ophiuchi and B40. Figure 1 shows the spatial (2D) distribution of early type stars based on HIPPARCOS observations. Overlayed are the areas covered by our ROSAT based study of young low-mass stars. The area designated US-A is centered on the core of Upper Scorpius, whereas the area designated US-B lies at the interface between Upper Scorpius and the older subgroup Upper Centaurus-Lupus. The exact coordinates of the area under study are summarized in the following:

1) $\alpha(2000) = 15^h24^m$ to 16^h00^m, $\delta(2000) = -35°$ to $-28°$
2) $\alpha(2000) = 15^h48^m$ to 16^h04^m, $\delta(2000) = -28°$ to $-23°$
3) $\alpha(2000) = 15^h48^m$ to 16^h04^m, $\delta(2000) = -23°$ to $-19°$

In addition to the RASS observations, several sets of pointed PSPC observations with exposure times up to 11 ksec were obtained and analyzed (Table 1).

The data reduction was done using the EXtended Scientific Analysis System (EXSAS, Zimmermann et al. 1994). In total, 303 individual X-ray sources were identified. 78 ROSAT sources had at least one late-type star with lithium absorption as an optical counterpart within the ROSAT error circle (see below). For the 8 sources with more than 300 counts it was possible to fit a Raymond-Smith spectrum (Raymond & Smith 1977) to the data, and to derive plasma temperatures T_X and hydrogen column densities N_H. For the majority of the sources, however, count rates were too low (see Table 2). In these cases, plasma temperatures and energy conversion factors were derived from hardness ratios assuming a Raymond-Smith spectrum. For the faintest sources in the sample, the uncertainties in the energy conversion factors derived from the hardness ratios were still too large, and we instead used an average energy conversion factor of 1.1×10^{-11} erg cm^{-2} (e.g. Neuhäuser et al. 1995).

Integrated counts, count rates, hardness ratios, plasma temperatures, X-ray luminosities, and angular separation between the centroid of the X-ray source and its stellar counterpart are summarized in Table 2. A column is included, indicating whether a source was detected in the RASS ("S") or in pointed observations ("P"). A few sources were only detected in the early reduction of the RASS, but not in a second, improved analysis. For these sources only upper limits on count rates and X-ray luminosities are given. The X-ray luminosity has been derived under the assumption of a distance of 145 pc (de Zeeuw et al. 1999). The correction for X-ray absorption is based on the relation N_H [cm^{-2}] $= 2.2\times10^{21} \times A_V$ [mag] (Jenkins & Savage 1974; Gorenstein 1975), where N_H denotes the hydrogen column density and A_V denotes the amount of visual extinction (see section 2.4). Hydrogen column densities derived from hardness ratios are more uncertain.

2.2. *Spectroscopic and photometric follow-up observations*

Optical counterparts to the X-ray sources were identified using the SIMBAD database, the Guide Star Catalogue, and Palomar Sky Survey plates. About 1/3 of the X-ray sources were identified as active galaxies, and were not further considered. Optical spectra of stars within the ROSAT error circle were obtained at La Silla, Chile, with the ESO 1.5m telescope and the ESO/MPI 2.2m telescope. In addition, standard stars for flux calibration and spectral classification were observed. The spectra cover the wavelength range from 520 nm to 780 nm with a resolution of 0.26 nm (2 pixel). The spectra were extracted and wavelength and flux calibrated using MIDAS[1]. Spectral types were determined based on the equivalent width of a number of diagnostic lines (Ca, Fe, Mg, Na) and a library of stars with known spectral types, which had been observed with the same instrumental set-up. We also measured the equivalent width of the Hα line (absorption or emission) and the lithium I 670.7 nm absorption line.

Stars with at least a tentative detection of the lithium line were also observed with the CCD cameras at the Dutch 90cm and the Danish 1.5m telescope, and the infrared photometer at the ESO 1m telescope. A log of the observations can be found in Table 3. Finding charts resulting from the CCD observations are presented in Figure 2.

The photometric reduction was carried out following standard procedures and using IRAF for the optical data and ESO software (SNOPY) for the infrared data. The photometric calibration is based on standard stars from the list by Landolt (1992) in the optical, and on standard stars from the ESO infrared standard star list (Bouchet

[1]Munich Image Data Analysis System

et al. 1991) in the infrared. Photometric uncertainties are of the order of 0.02 mag to 0.08 mag in the optical, and around 0.02 mag to 0.04 mag in the infrared. The results of the photometry are summarized in Table 4.

Radial and rotational velocities ($v \sin i$ values) of a subsample of the stars were measured with CORAVEL (Baranne, Mayor, & Ponchet 1979) at the Danish 1.5m telescope. Data reduction was carried out following the standard procedures. The results of the CORAVEL observations are summarized in Table 5. There is a good agreement with the values determined by Walter et al. (1994) for stars in the overlapping sample.

Table 6 lists the coordinates of the stars in the ROSAT sample.

2.3. *Additional space-based observations*

As part of a search for substellar companions to T Tauri stars, eleven of the stars in the present sample were observed with HST/NICMOS. In addition to a number of faint companions, the observations also revealed several previously unknown close companions and hierarchical triple systems (see Table 7).

Eleven stars from the present sample were also observed with the Infrared Space Observatory (ISO) and ISOCAM at 6.7 μm, and 15 μm with the aim to search for excess emission from faint circumstellar disks (Moneti et al. 1999). A more detailed analysis of the HST and ISO data will be presented by Brandner et al. (in prep.).

2.4. *Determination of effective temperature and luminosity*

In order to place stars on an HR-diagram and compare them with theoretical evolutionary tracks, the effective temperatures and luminosities of the stars have to be determined. Because the surface gravity of T Tauri stars is lower than that of dwarfs by a factor of 2 to 10, ideally one would like to rely on calibrations for luminosity class IV objects. Subgiants, however, are poorly studied, and no comprehensive, unique compilation of their intrinsic colors and spectral type–effective temperature relations is available. Therefore, the following analysis is based on the compilation of colors, bolometric corrections, and effective temperatures for late-type dwarfs as a function of spectral type by Hartigan, Strom, & Strom (1994). As T Tauri stars very often show UV- and IR-excesses, the in general excess-free V–I color index was used to compute the visual extinction. A fixed distance of 145 pc to each star was assumed in order to derive the luminosity. In addition to the stars in the ROSAT sample, we also recomputed effective temperatures and luminosities for the stars in the EINSTEIN sample by Walter et al. (1994) and merged them with our sample. Table 6 summarizes the physical properties of the stars. The visual extinction values were then used to calculate the extinction in the X-rays, as hydrogen column densities derived directly from the X-ray data are highly uncertain (see above).

3. RESULTS

3.1. *HR-Diagram*

Figure 3 shows all stars in the present sample placed on an HR-diagram assuming intrinsic colors of main-sequence stars and a distance of 145 pc (de Zeeuw et al. 1999). Overplotted are evolutionary tracks and isochrones from Palla & Stahler (1999). The HR-diagram exhibits a number of interesting features and pecularities:

i) There appears to be a clear correlation between effective temperature and stellar age in the sense that later type stars appear to be younger than earlier type stars. Apparently, Walter et al. (1994) noticed a simliar trend in their data. They concluded that intrinsic colors for T Tauri stars are different from dwarf colors, and used their data set to iteratively solve for both the unknown intrinsic colors and extinction.

ii) A number of stars appear to have ages below 500,000 yr. These stars, however, do not show the spectroscopic signatures typical for stars of that age such as strong Balmer line emission, veiling, or extreme UV- and IR-excess.

iii) Two stars (RXJ 1544.2-3117 and RXJ 1545.5-3249) appear to be located *below* the main-sequence. This indicates that the luminosity of at least some of the stars has been underestimated, and that these stars are actually at distances *larger* than 145 pc.

3.1.1. *Multiple Systems - Selection bias*

High-spatial resolution imaging (Ghez, Neugebauer, & Matthews 1993; Brandner et al. 1996; Köhler 1997; Köhler et al. 2000; Brandner et al., in prep.) and radial velocity observations (Walter et al. 1994; this paper) of the stars in the present sample reveal that at least 48 (41%) are binary or multiple systems. The distribution of stars in Figure 3 is strongly biased by this fact, as all multiple systems with separations less than 3″ are shown as unresolved systems. Figure 4 indicates which stars have been resolved as binary stars with separations less than 3″ by means of high-resolution imaging. As predicted by Simon, Ghez, & Leinert (1994) and first demonstrated for classical T Tauri stars by Brandner & Zinnecker (1997), unresolved binaries lead to an overestimate of the luminosity and thus an underestimate of the age of a stellar population. For each spectral type in our sample, we find the "unresolved" (sep. $\leq 3''$) binaries preferentially among the brightest stars. Thus, even if a distance of 145 pc is correct for most of the stars, the low-mass stars appear to be significantly older than the age of 1 to 2 Myr derived by Walter et al. (1994).

The high incidence of binary and multiple systems at each spectral type preferentially among the brighter stars indicates the presence of a selection effect in favor of multiple systems. The X-ray sample, in particular the stars identified in the RASS is flux limited. Unresolved binary and multiple systems are on average brighter than single objects, and are thus picked up in large numbers by the RASS (see Brandner et al. 1996 for a more detailed discussion of this selection bias). Compared to other nearby star forming regions, this selection bias is most pronounced in Scorpius-Centaurus because of the relatively short RASS exposure times around 500s, and the higher age of the stars (lower intrinsic X-ray luminosity).

In a study of the binary properties of the young stars in the X-ray selected sample, Brandner & Köhler (1998) found that the distribution of binary separations varies between US-A and US-B. For binary T Tauri stars located in the direction of an older subgroup (US-B) but not closely associated with early-type stars, the peak in the distribution of binary separations is at 215 A.U., whereas for bi-

nary T Tauri stars closely associated with the early-type stars in Upper Scorpius (US-A), the peak in the distribution is at 90 A.U. Brandner & Köhler (1998) speculate that the difference in the distribution of binary separations might reflect physical differences in the parental molecular cloud at the time star formation took place.

3.1.2. *HIPPARCOS parallaxes*

Eight of the brightest stars in our sample were also observed by the HIPPARCOS satellite, and meaningful parallaxes (S/N>3) were derived for all of them (Table 8). Two of the eight stars are at approximately the assumed distance of 145 pc, whereas the remaining six stars are considerably closer at distances ranging from only 40 pc to 90 pc. This implies that each of these stars has a lower luminosity than initially assumed for a distance of 145 pc. As a consequence, actual ages are a factor of 2 to 67 higher, and the actual masses are only 50% to 75% of the initial estimate (see Table 8 and Figure 5).

As parallaxes are only available for 8 of the 118 sources, we cannot generalize the results. It is clear, however, that ages and masses derived from the location in an HR-diagram are highly uncertain for the spatially widely scattered sample of X-ray active late-type stars in Scorpius-Centaurus. Hence, the conclusions regarding age and mass distribution of low-mass in Upper Scorpius by Walter et al. (1994) should be treated with caution. Preibisch & Zinnecker (1999) tried to take the effect of unresolved binary stars into account. It is, however, not clear if their assumption of a random pairing of the masses of binary components is justified. Similarly, the HIPPARCOS parallaxes hint that the X-ray selected sample might be biased towards the most nearby members of the association.

Table 4 indicates that a large fraction of the present sample would have been bright enough for observations with HIPPARCOS. The HIPPARCOS Input Catalogue (HIC), however, was only complete to V=7mag. The large number of bright early-type stars in Scorpius-Centaurus (see, e.g., de Geus et al. 1989, and Figure 3) prevented the inclusion of all but a few of the brightest late-type stars from the present sample. A more detailed study of parallaxes and proper motions of low-mass stars in Scorpius-Centaurus has to wait until the first results from the next astrometric satellite mission will become available.

Hence, for the moment it is advisable to restrict further studies of the physical characteristics of the present sample to the distance independent physical properties, such as spectral features, or the ratio of X-ray luminosity to bolometric luminosity (L_X/L_{bol}).

3.2. *Lithium equivalent width and evolutionary status*

One of the spectral features is the lithium equivalent width. In young low-mass stars, the lithium abundance varies with age and spectral type (Herbig 1965; Bodenheimer 1965). Martín (1997, 1998) suggested a diagnostic diagram to distinguish weak-line T Tauri stars (WTTS) from more evolved ("Post") T Tauri stars (PTTS). Classical T Tauri stars (CTTS) are classified based on the equivalent width of the Hα emission line and their spectral type. For late spectral types larger equivalent widths are required in order to distinguish CTTS from dMe stars.

In the diagnostic diagram the lithium equivalent width W_{Li} is plotted against the effective temperature (see Figure 6). The typical location of WTTS and stars in Young Open Clusters (Hyades, Pleiades) is indicated. PTTS are located between WTTS and Young Open Cluster stars. It is important to note that the current definition of PTTS according to Martín (1997, 1998) includes evolved (lithium deficient) T Tauri stars, which are still on their Hayashi tracks, and true *post* T Tauri stars (in the sense as originally postulated by Herbig (1978), i.e., past the Hayashi phase). In addition, for young stars with spectral type K7 or later, the location of the dividing line between WTTS and PTTS might be somewhat arbitrary.

According to the definition by Martín (1997, 1998), 7 of the stars in our sample would be classified as CTTS, 20 as WTTS, 49 stars as PTTS[2], and 42 would remain unclassified. The unclassified ("ambiguous") stars fall into a region which is occupied both by pre-main sequence stars and young main-sequence stars. Resolved binary stars and unresolved ("single") stars show no statistically significant difference in the number ratios of WTTS to PTTS. Very interesting is the high incidence of PTTS in Upper Scorpius with 2.5 times more PTTS than WTTS. Applying the same criteria to the 78 X-ray active late-type stars studied by Preibisch et al. (1998) in the northern part of Upper Scorpius and Ophiuchus, results in 1 CTTS, 21 WTTS, and 9 PTTS. 47 stars remain unclassified. The survey by Preibisch et al. (1998) was on average one magnitude less sensitive than the present survey and also included larger areas of the neighboring Ophiuchus molecular clouds. Consequently, only 21% of the 57 X-ray selected stars with spectral classification in the sample by Preibisch et al. are of spectral type M, whereas 53% of the 118 stars in our sample are M-stars.

In a similar study, Martín et al. (1998), find 7 WTTS for every PTTS in their X-ray (ROSAT) selected sample of the ρ Ophiuchi star forming region. Figure 7 shows the spatial distribution of CTTS (plus signs), WTTS (open diamonds), and PTTS (crosses) in Upper Scorpius and Ophiuchus. Small dashed rectangles indicate pointings by the EINSTEIN satellite (Walter et al. 1994), dashed circles and larger rectangles mark areas studied by pointed ROSAT observations and by the ROSAT All Sky Survey. There is a clear spatial separation between WTTS and PTTS. WTTS tend to cluster near ρ Ophiuchi and B40, whereas PTTS are distributed almost homogeneously throughout the entire area under study.

A scatter in the equivalent widths of stars with the same spectral type in young open clusters indicates that lithium abundances depend on additional parameters. Possible parameters are chemical inhomogeneities in star forming regions and stellar rotation. Young stars rotate considerably faster than the present day Sun (e.g. Bouvier et al. 1993), which leads to stronger magnetic fields via the dynamo-effect. The presence of magnetic fields could aggravate convection and thus significantly inhibit the depletion of lithium (Ventura et al. 1998), making the lithium abundance an imprecise age indicator unless the rotational history of a star can be reconstructed.

[2]RXJ 1545.8-3020 of spectral type K3 might also be classified as a WTTS. Martín (1998) quote minimum lithium equivalent widths only for spectral types K2 and K5, and RXJ 1545.8-3020's lithium equivalent width falls in between.

3.3. *Activity indicators: X-ray and Hα*

Figure 8 indicates that stars with lower effective temperatures tend to have a higher ratio of X-ray luminosity to bolometric luminosity. This has also been observed for young stars within 25 pc of the sun (e.g., Sterzik & Schmitt 1997). WTTS and PTTS show a similar behavior. There is also a clear correlation between the Hα equivalent width and the ratio of X-ray luminosity to bolometric luminosity (Figure 9). This suggests that the majority of the stars in the present sample have active coronae and chromospheres, which are responsible for the X-ray flux and the Hα emission. Again PTTS and WTTS show a very similar behavior. Only the CTTS clearly deviate from this relation. Here ongoing accretion is very likely responsible for the larger Hα equivalent widths.

3.4. *Rotational velocities*

The rotational velocity of a star is a further indicator of its age. The rotational velocity, however, is also a function of the initial angular momentum and the accretion history of the star. For young stars the transport of angular momentum between a circumstellar disk and the star (and possibly a bipolar outflow) is of importance. Table 5 lists v sin i and radial velocities as measured for a subsample of all stars. Figure 10 shows the ratio of X-ray luminosity to bolometric luminosity plotted against v sin i for CTTS, WTTS, PTTS, and the unclassified stars. PTTS tend to have v sin i values between 0 and 20 $\mathrm{km\,s^{-1}}$, whereas WTTS tend to have v sin i values between 15 to 40 $\mathrm{km\,s^{-1}}$. Unclassified X-ray active stars show a range in v sin i values between 0 $\mathrm{km\,s^{-1}}$ and 70 $\mathrm{km\,s^{-1}}$. PTTS clearly stand out with their on average very low v sin i values, suggesting that they are older than the WTTS (see, e.g., Herbig 1978).

There is no clear correlation between Hα equivalent width and v sin i values. The unclassified stars tend to have the smallest Hα equivalent widths and the largest spread in v sin i values. There is also no apparent correlation between the lithium equivalent width and v sin i values.

4. SUMMARY

Based on ROSAT observations and data obtained with ground-based telescopes, we have carried out an extensive study of the low-mass pre-main-sequence population in Upper Scorpius, the youngest subgroup of the Scorpius-Centaurus OB association. In this data paper we presented the observations, and a preliminary analysis and interpretation of the results.

Combined with a previous study of Upper Scorpius by Walter et al. (1994) a total of 118 X-ray active late-type stars with at least traces of lithium absorption in their spectra could be identified. An attempt to place the stars in an HR-diagram in order to derive masses and ages is problematic for two reasons:

First, high-resolution imaging and spectroscopy reveal a high incidence of binary and multiple systems. This bias can be attributed to the flux-limited character of the X-ray surveys. Deriving the evolutionary status for the unresolved systems from their position in an HR-diagram would lead to an overestimate of the mass and an underestimate of the age of the population of young X-ray active late-type stars in Upper Scorpius.

Secondly, HIPPARCOS parallaxes for a small subset reveal a spread in distances by at least a factor of 2, which makes luminosity estimates uncertain by a factor of 4 if a fixed distance is assumed for all the stars in the sample. We conclude that ages and masses for X-ray active late-type stars in Upper Scorpius cannot reliably be derived unless multiplicity and distance uncertainties are properly taken into account. Previous studies either neglected or underestimated this effects, which led to an underestimate of the age of the late-type stellar population in Upper Scorpius.

Distance independent indicators can be used to study the evolutionary status. We find a clear correlation between the ratio of the X-ray to bolometric luminosity and the Hα equivalent width which suggests the presence of active coronae and chromospheres in these stars. An analysis of the spectral properties reveals that 7 stars in the sample can be classified as classical T Tauri stars (CTTS), 20 as weak-line T Tauri stars (WTTS), 49 as post-T Tauri stars (PTTS), and 42 stars remain unclassified. Furthermore, CTTS and WTTS cluster near ρ Oph and B40, whereas PTTS are spread out over the entire area under study. The majority of low-mass stars in Upper Scorpius appears to be at least as old as the B-type stars. Star formation ceased after the formation of the high-mass stars. If the amount of photospheric lithium is an age indicator, then there is a clear trend with the late-type stars close to Upper Centaurus-Lupus being the oldest, followed by the late-type stars in Upper Scorpius and the ρ Ophiuchi star forming region.

The larger degree of lithium depletion in PTTS compared to WTTS might be related to the higher age of the PTTS and/or a smaller initial angular momentum.

The sample of 49 genuine post-T Tauri stars should prove valuable for future studies of the timescales of disk evolution and planet formation around young solar-type stars.

Discussions with Gibor Basri, Sabine Frink, George H. Herbig, Rainer Köhler, and Eduardo Martín are gratefully acknowledged. MK and HZ acknowledge support by the Deutsche Forschungsgemeinschaft (DFG) and the Verbundforschung der Deutsche Agentur für Raumfahrtangelegenheiten (DARA) under grant number 05 OR 9103 0. WB acknowledges support by NASA through grant number GO-07412.01-96A from the Space Telescope Science Institue, which is operated by the Association of Universities for Research in Astronomy, Inc., under NASA contract NAS5-26555. The ROSAT project was supported by the Bundesministerium für Bildung, Wissenschaft, Forschung und Technologie (BMBF/DLR) and the Max-Planck-Society.

REFERENCES

Baranne, A., Mayor, M., Ponchet, J.L. 1979, Vistas in Astron., 23, 279

Blaauw, A. 1991, in *The Physics of Star Formation and Early Stellar Evolution*, ed. C.J. Lada & N.D. Kylafis (Dordrecht: Kluwer), 125

Bodenheimer, P. 1965, ApJ, 142, 451

Bouchet, P., Schmider, F.X., Manfroid, J. 1991, A&AS, 91, 409

Bouvier, J., Cabrit, S., Fernandez, M., Martín, E.L., Matthews, J.M., 1993, A&A, 272, 176

Brandner, W., Alcalá, J. M., Kunkel, M., Moneti, A., Zinnecker, H. 1996, A&A, 307, 121

Brandner, W., Köhler, R. 1998, ApJ, 499, L79

Brandner, W., Zinnecker, H. 1997, A&A, 321, 220

de Geus, E.J., de Zeeuw, P.T., Lub, J. 1989, A&A, 216, 44

de Zeeuw, P.T., Hoogerwerf, R., de Bruijne, J.H.J., Brown, A.G.A., Blaauw, A. 1999, AJ, 117, 354

Ghez, A.M., Neugebauer, G., Matthews, K. 1993, AJ, 106, 2005

Gorenstein, P. 1975, ApJ, 198, 95

Hartigan, P., Strom, K.M., Strom, S.E. 1994, ApJ, 427, 961

Herbig, G.H. 1965, ApJ, 141, 588

Herbig, G.H. 1978, in Problems of Physics and Evolution of the Universe, Academy of Sciences of Armenian SSR, ed. L.V. Mirzoyan, p. 171

Jenkins, E.B., Savage, B.D. 1974, ApJ, 187, 243

Köhler, R. 1997, PhD Thesis, Universität Heidelberg

Köhler, R., Kunkel, M., Leinert, Ch., Zinnecker, H. 2000, A&A, in press

Landolt, A.U., 1992, AJ, 104, 372

Mathieu, R.D., Walter, F.M., Myers, P.C. 1989, AJ, 98, 987

Martín, E.L., 1997, A&A, 321, 492

Martín, E.L., 1998, AJ, 115, 351

Martín, E.L., Montmerle, T., Gregorio-Hetem, J., Casanova, S., 1998, MNRAS, 300, 733

Moneti, A., Zinnecker, H., Brandner, W., Wilking, B. 1999, in "Astrophysics with Infrared Surveys: A Prelude to SIRTF", ASP Conf. Series 117, eds. M.D. Bicay, C.A. Beichman, R.M. Cutri, B.F. Madore, p. 355

Neuhäuser, R., Sterzik, M., Schmitt, J.H.M.M., Wichmann, R., Krautter, J. 1995, A&A, 297, 391

Neuhäuser, R., Brandner, W. 1998, A&A, 330, L29

Palla, F., Stahler, S. 1999, ApJ, 525, 772

Poeppel, W. 1997, Fund. of Cosmic Phys., 18, 1

Preibisch, T., Guenther, E., Zinnecker, H. et al. 1998, A&A, 333, 619

Preibisch, T., Zinnecker, H. 1999, AJ, 117, 2381

Raymond, J.C., Smith, B.W., 1977, ApJS, 35, 419

Simon, M., Ghez, A.M., Leinert, Ch., 1993, ApJL, 408, 33

Sterzik, M., Schmitt, J.H.M.M. 1997, AJ, 114, 1673

Trümper, J. 1983, Adv. Space Res. 2, No 4, 241

Ventura, P., Zeppieri, A.,Mazzitelli, I., D'Antona, F. 1998, A&A, 331, 1011

Walter, F.M., Vrba, F.J., Mathieu, R.D., Brown, A., Myers, P.C. 1994, AJ, 107, 692

Zimmermann, H.U., Becker, W., Belloni, T. et al., 1994, *EXSAS User's Guide*, MPE Report

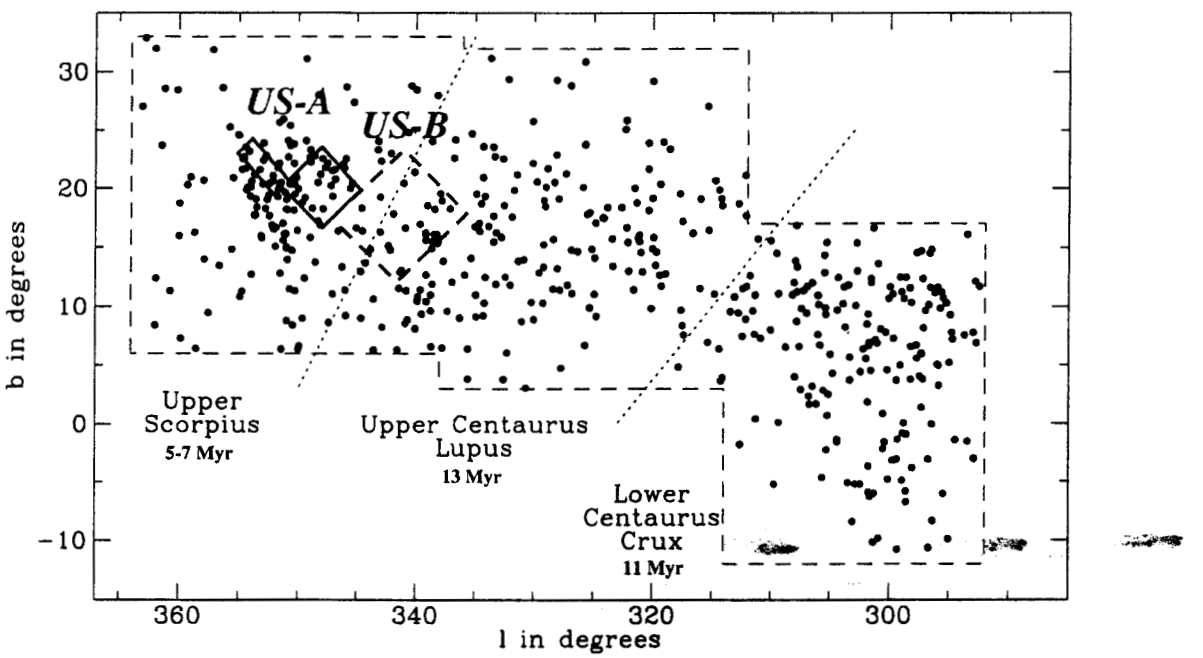

FIG. 1.— Location of our survey area ("US-A", "US-B") with respect to the ScoCen OB association. The underlying plot shows the distribution of early-type stars in ScoCen and is based on HIPPARCOS observations (adapted from de Zeeuw et al. 1999).

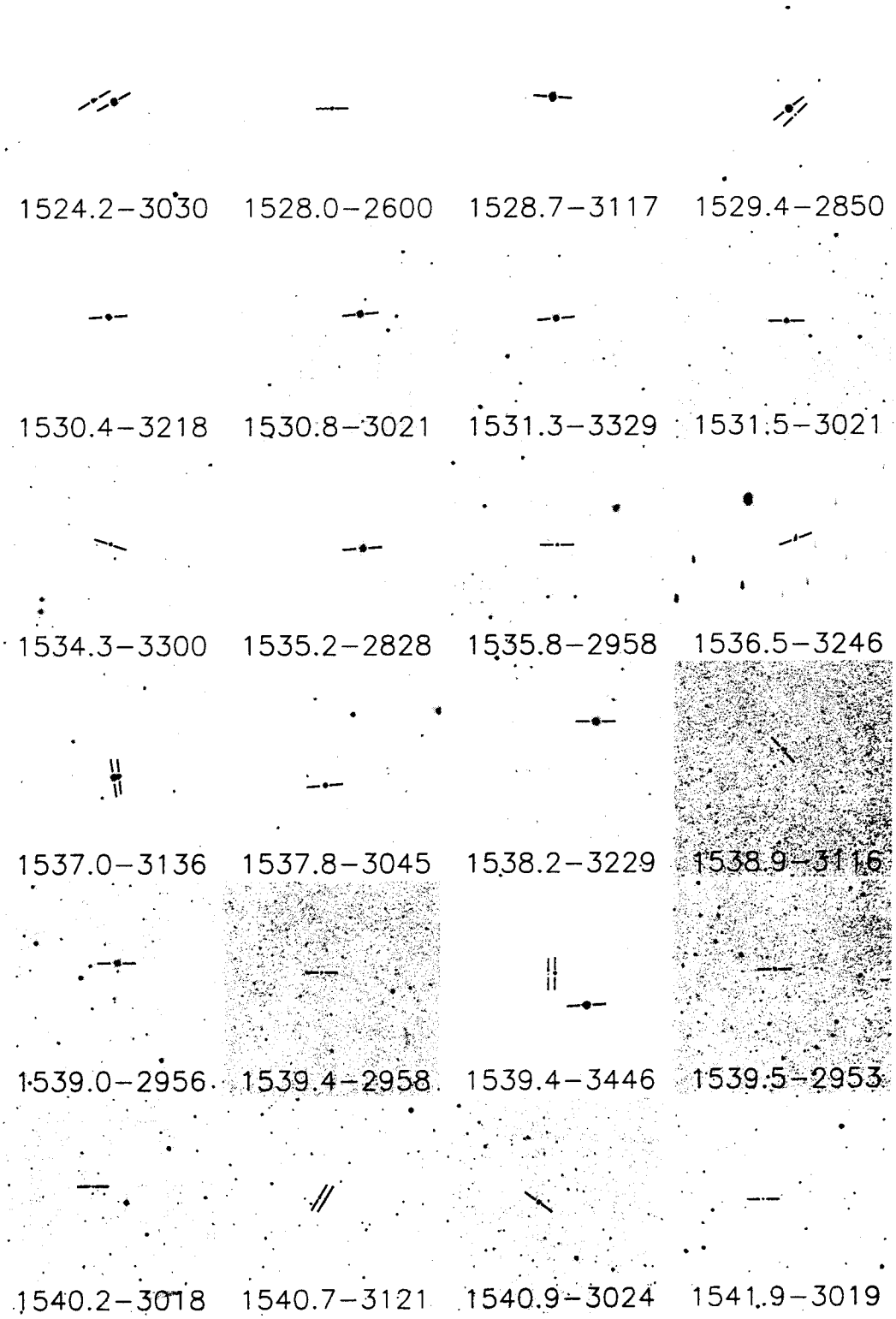

FIG. 2.— Visual finding charts for X-ray active young stars in Upper Scorpius. The field of view is 3′.5 × 3′.5. North is to the top and east is to the left.

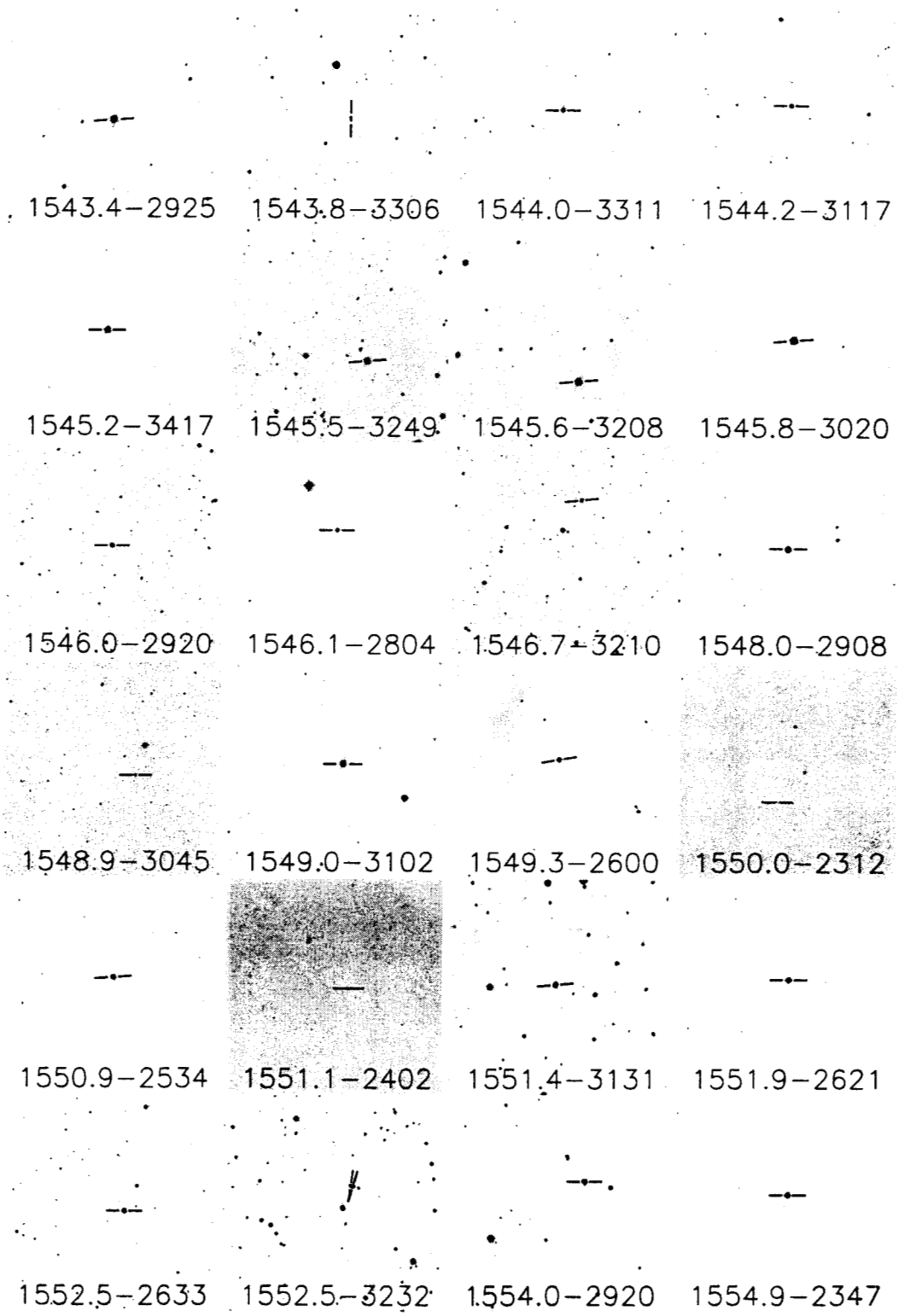

FIG. 2.— (continued) Visual finding charts for X-ray active young stars in Upper Scorpius. The field of view is 3′.5 × 3′.5. North is to the top and east is to the left.

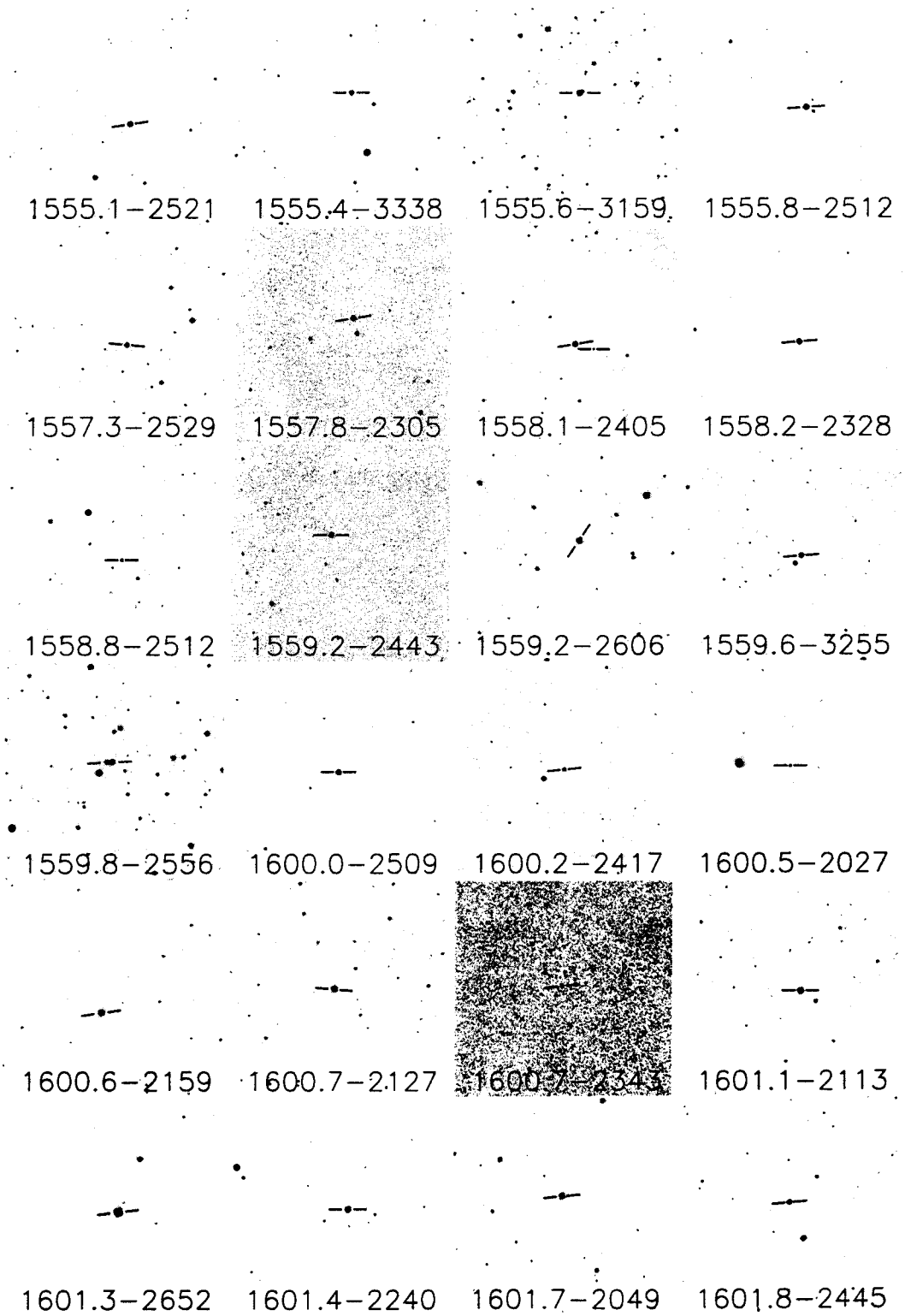

FIG. 2.— (continued) Visual finding charts for X-ray active young stars in Upper Scorpius. The field of view is 3.′5 × 3.′5. North is to the top and east is to the left.

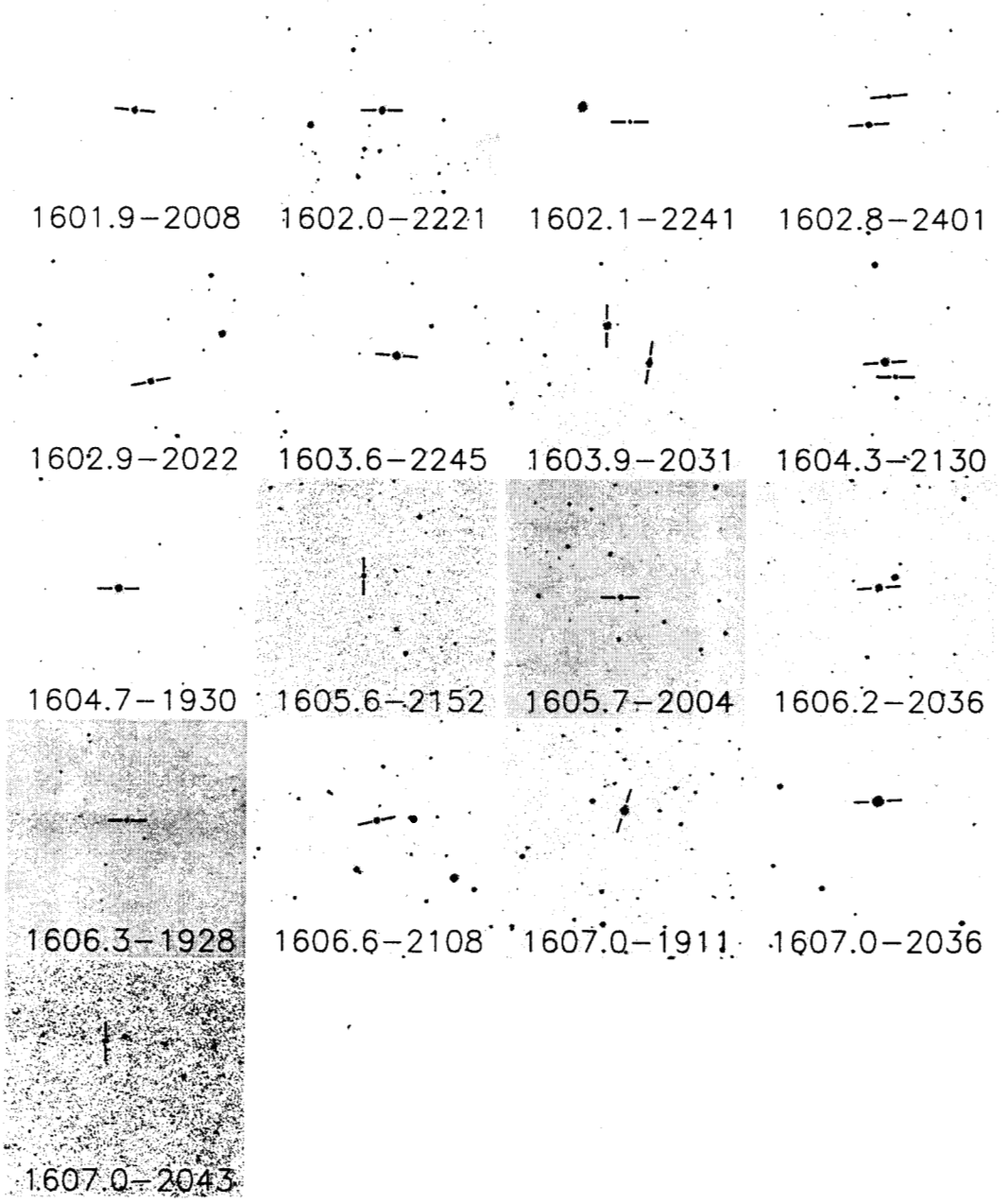

FIG. 2.— (continued) Visual finding charts for X-ray active young stars in Upper Scorpius. The field of view is 3′.5 × 3′.5. North is to the top and east is to the left.

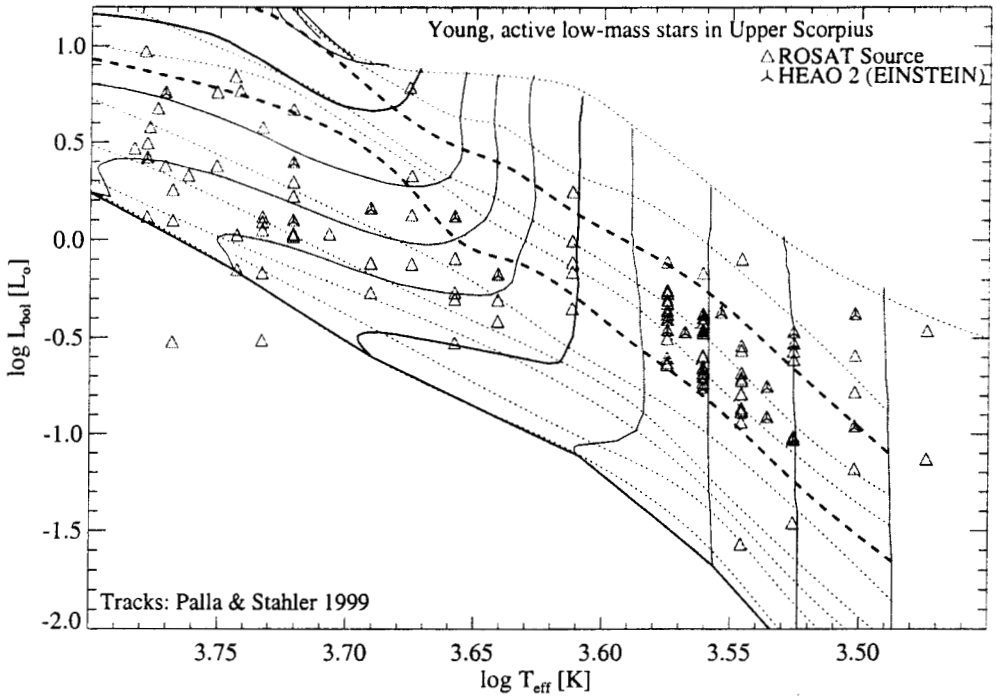

FIG. 3.— HR-diagram of X-ray active low-mass stars detected by ROSAT and HEAO 2 (EINSTEIN satellite) assuming a distance of 145 pc. Isochrones for 1 Myr and 5 Myr are shown as thicker dashed lines, and the evolutionary tracks for $0.8\,M_\odot$ and $2.0\,M_\odot$ are shown as bold lines.

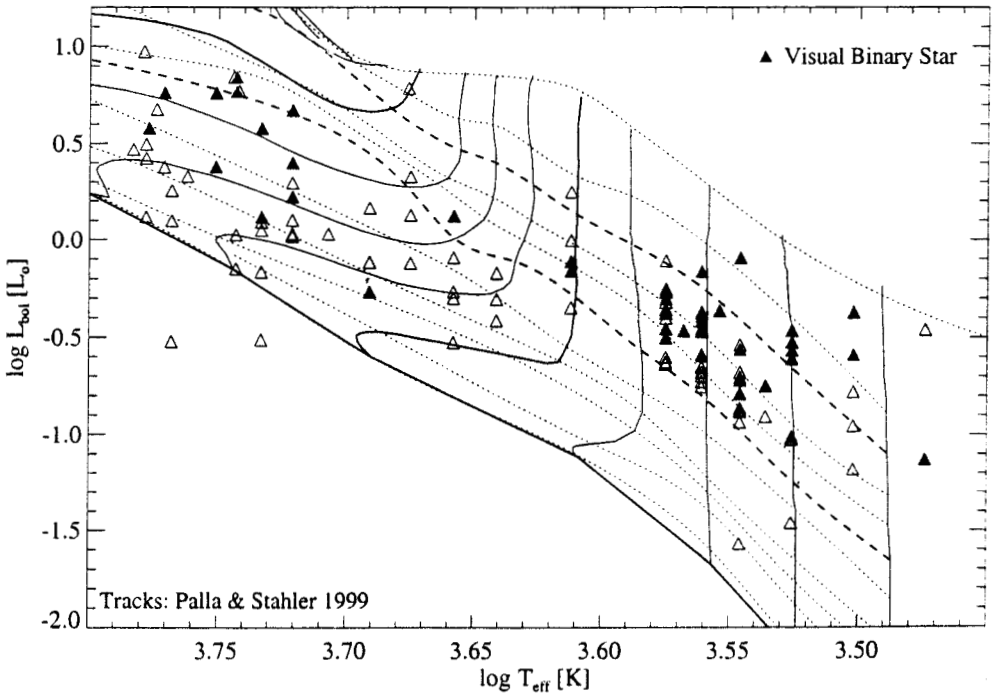

FIG. 4.— HR-diagram. Visual binaries are indicated by filled triangles. Note the high incidence of visual binaries among the brightest stars for each spectral type, which strongly biases the age and mass estimates for the ensemble. Isochrones for 1 Myr and 5 Myr are shown as thicker dashed lines, and the evolutionary tracks for $0.8\,M_\odot$ and $2.0\,M_\odot$ are shown as bold lines.

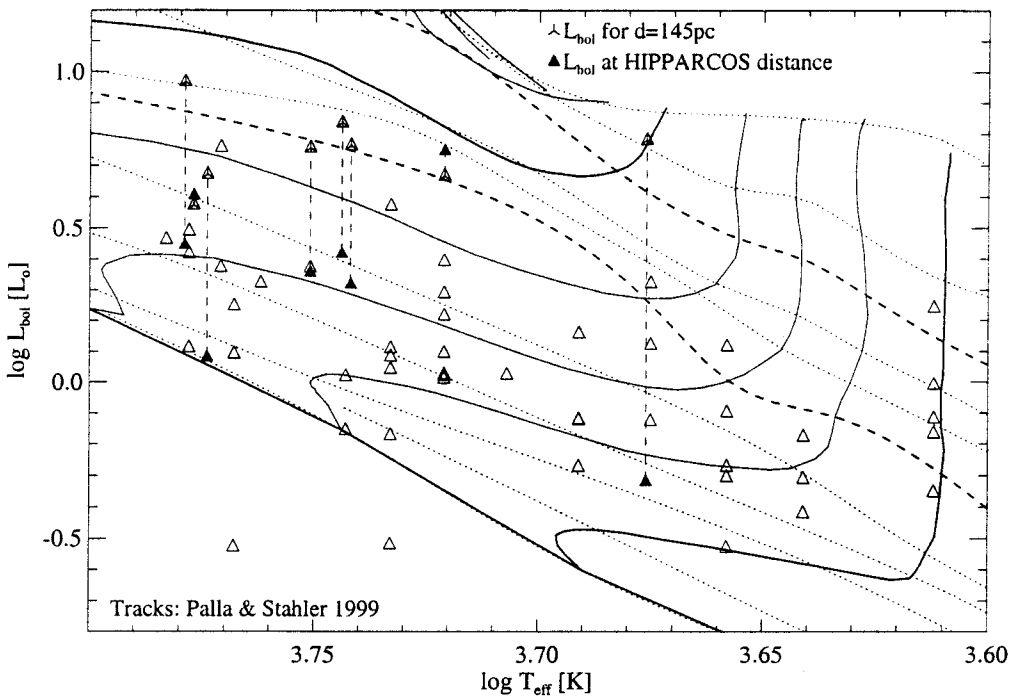

FIG. 5.— HR-diagram showing the effect of an initially false distance estimate of 145 pc to some of our sample stars. Stars with HIPPARCOS parallaxes have been shifted along the dashed line to the appropriate luminosity. Isochrones for 1 Myr and 5 Myr are shown as thicker dashed lines, and the evolutionary tracks for 0.8 $M_\odot$ and 2.0 $M_\odot$ are shown as bold lines.

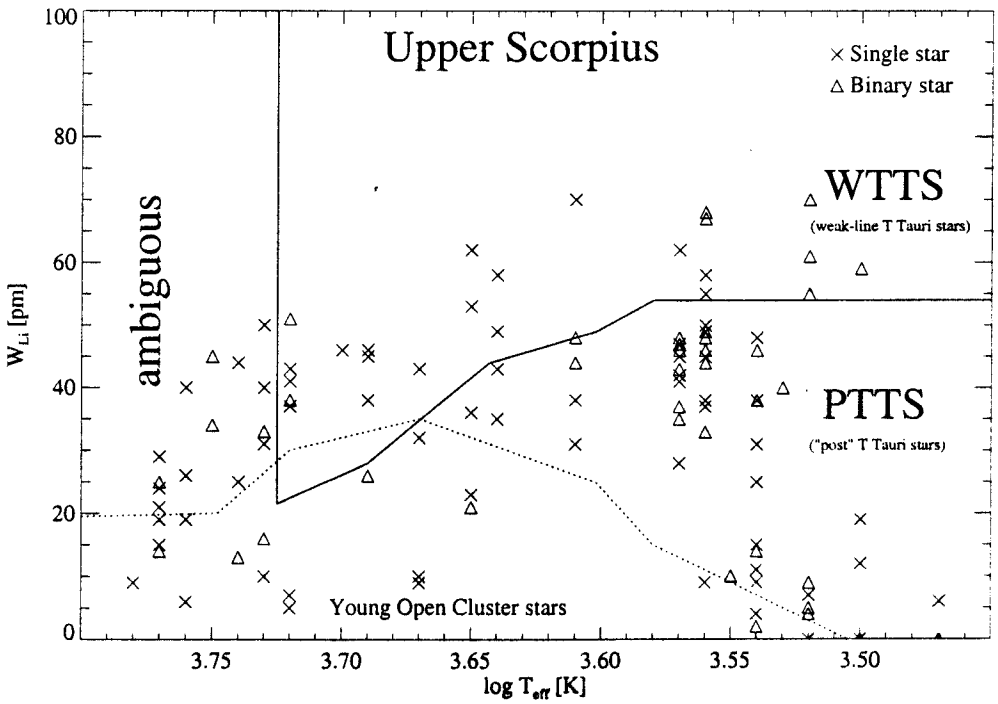

FIG. 6.— Diagnostic diagram of lithium equivalent width vs. effective temperature. This type of diagram allows one to distinguish between WTTS and PTTS (Martín 1997). Interesting is the large number of PTTS in Upper Scorpius.

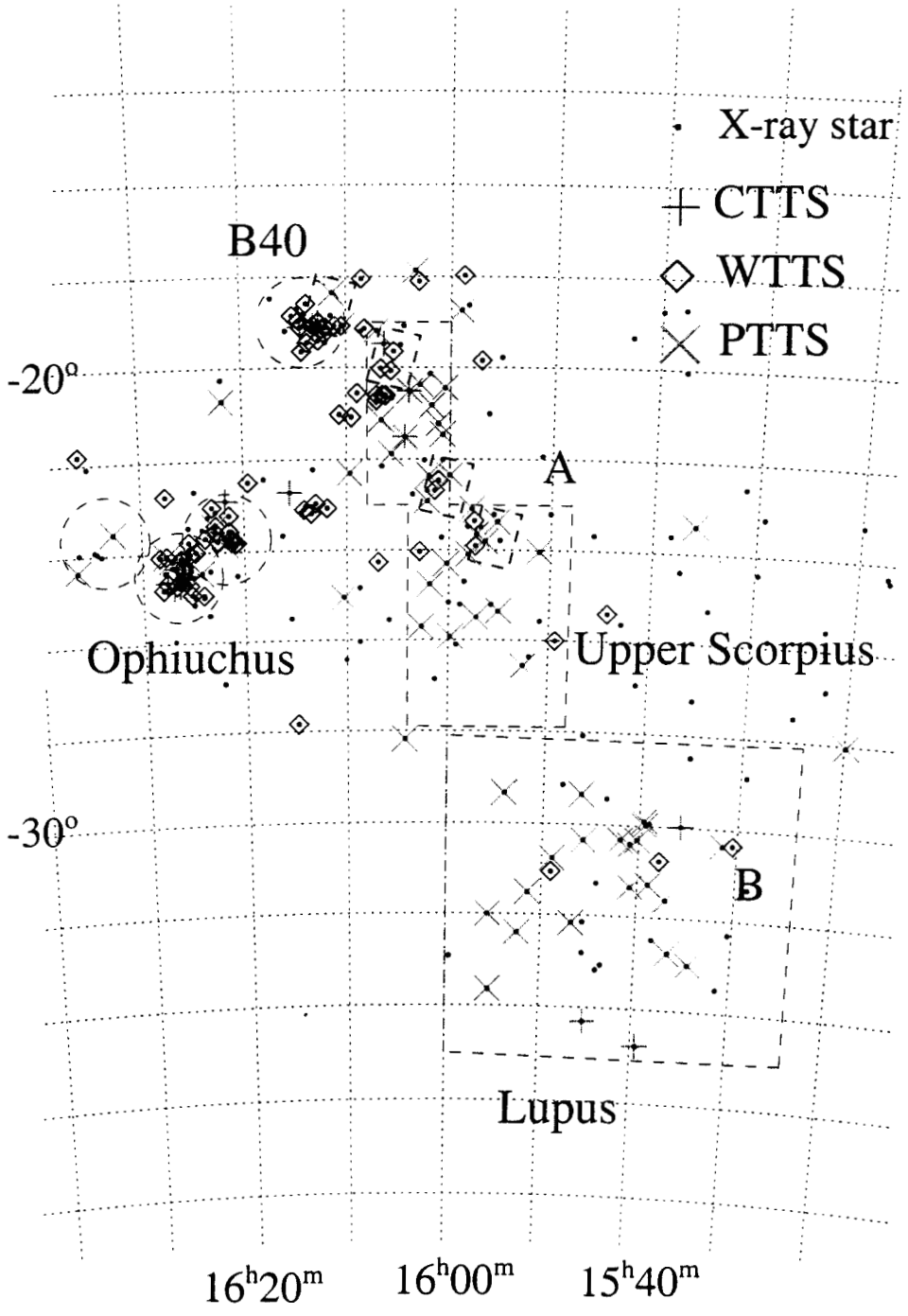

FIG. 7.— Spatial distribution of X-ray active stars in Upper Scorpius and Ophiuchus (dots). CTTS, WTTS, and PTTS are marked with plus signs, open diamonds, and crosses, respectively. Regions around the dark clouds in ρ Oph and B40 have a higher density of WTTS. Shown are stars from our ROSAT sample and from the studies by Walter et al. (1994), Martín et al. (1998), and Preibisch et al. (1998).

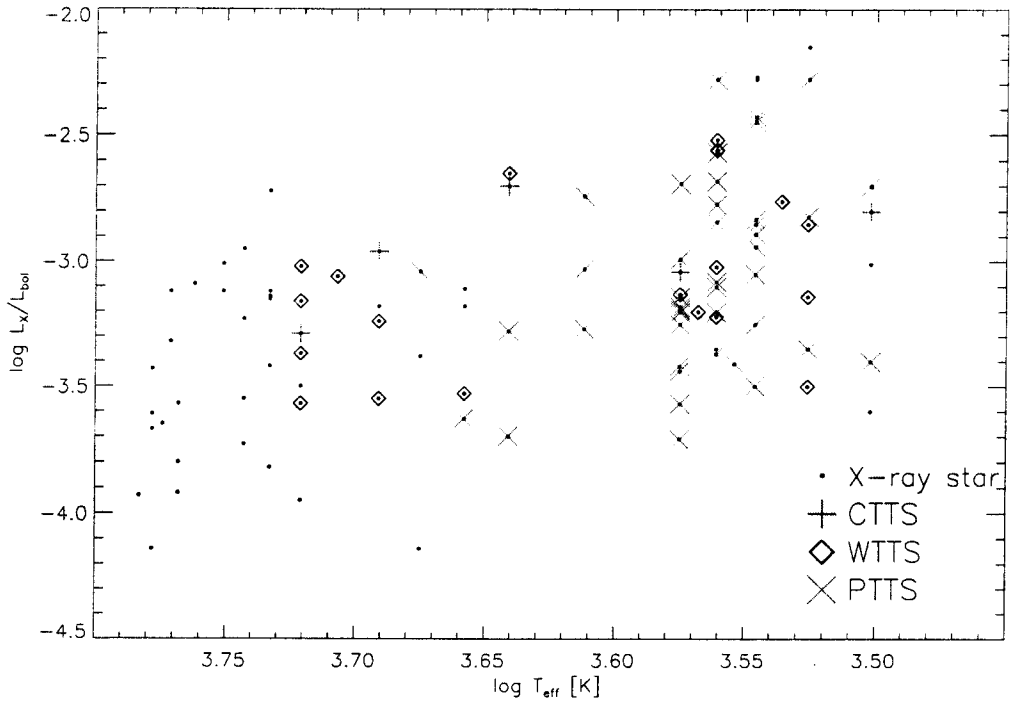

FIG. 8.— Ratio of X-ray luminosity to bolometric luminosity vs. effective temperature for X-ray active stars in Upper Scorpius. Stars with lower effective temperature tend to have a higher L_X/L_{bol}.

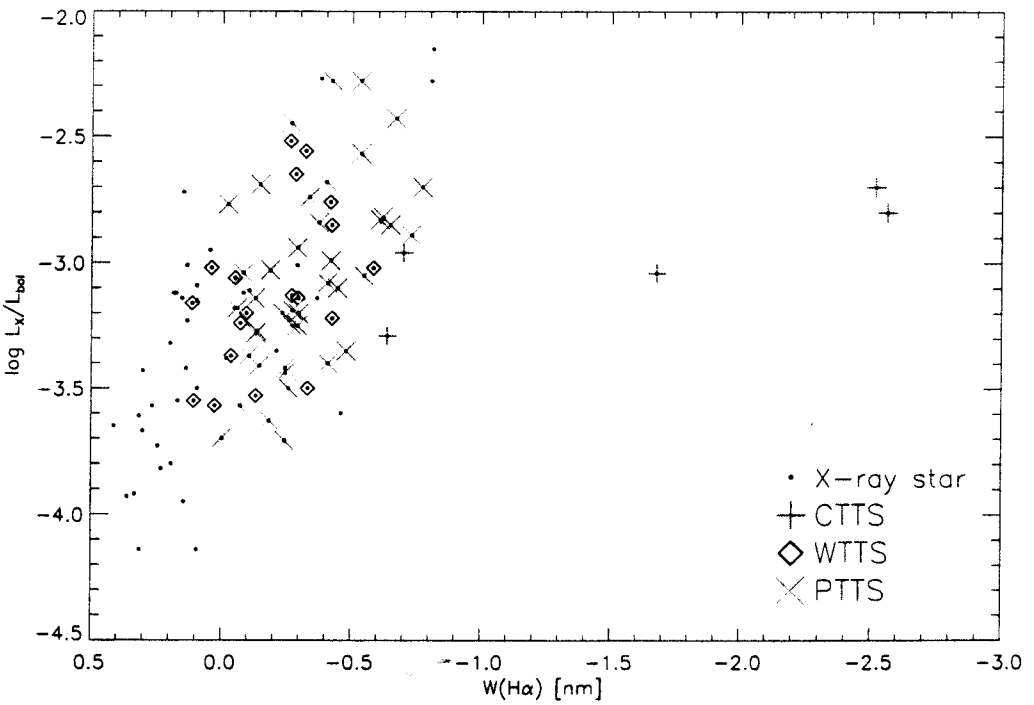

FIG. 9.— Ratio of X-ray luminosity to bolometric luminosity vs. Hα equivalent width. There is a clear correlation between the X-ray activity and the Hα equivalent width which suggests a correlation between coronal and chromospheric activity. CTTS fall outside this relation with their larger Hα equivalent width due to ongoing accretion.

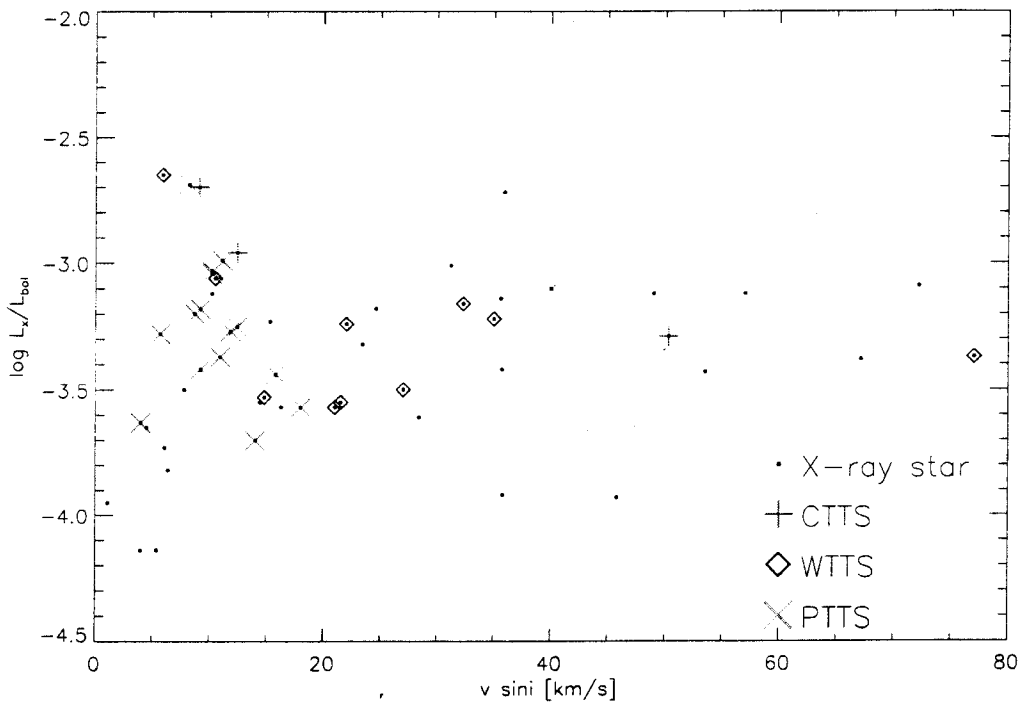

FIG. 10.— Ratio of X-ray luminosity L_X to bolometric luminosity L_{bol} vs. v sin i. L_X/L_{bol} shows no clear dependence on v sin i. This might, however, be in part due to a selection effect, as many of the stars with log L_X/L_{bol} > -3.0 do not have a v sini measurement. PTTS rotate on average slower (0-20km/s) than WTTS (15-40km/s), which suggests that the PTTS are older than the WTTS. Unclassified stars exhibit the largest spread in v sin i.

TABLE 1
LOG OF POINTED ROSAT PSPC OBSERVATIONS OF THE UPPER SCORPIUS REGION

Name	Date	RA (2000) [hms]	DEC (2000) [° ′ ″]	exp. time [s]
US 1	1992 Aug 23	15 37 28.7	-31 20 24	4257
US 2	1992 Aug 21	15 39 26.3	-30 12 55	2448
US 2	1993 Feb 03	15 39 26.3	-30 13 12	1890
US 3	1992 Aug 24	15 41 00.0	-32 16 12	4476
US 4	1992 Aug 24	15 43 00.0	-31 08 24	4139
US 5	1992 Aug 25	15 44 52.7	-30 01 12	4545
US 6	1992 Feb 27	15 46 38.4	-32 03 36	3538
US 6	1993 Aug 09	15 46 38.4	-32 03 36	1181
US 7	1992 Aug 29	15 48 31.2	-30 55 48	4440
3 SCO[1]	1992 Feb 09	15 54 38.3	-25 14 24	8967
HR 5942[1]	1992 Mar 07	15 58 35.9	-24 49 48	10764
HD 142361[1]	1993 Feb 27	15 54 59.9	-23 47 24	3352
HD 142361[1]	1993 Aug 18	15 54 59.9	-23 47 24	1853

NOTE.—[1] archive data

TABLE 2
RESULTS OF ROSAT OBSERVATIONS. S/P INDICATES IF A SOURCE HAS BEEN DETECTED IN THE RASS ("S") OR IN POINTED OBSERVATIONS ("P").

RX J	counts	count rate [s^{-1}]	HR 1	HR 2	log T_X [K]	log L_X [erg/s]	S/P	sep. ["]
1524.2–3030	23.3± 7.8	0.043± 0.014	0.50± 0.29	−0.26± 0.34	$6.46^{+0.25}_{-0.05}$	$30.41^{+0.31}_{-0.45}$	S	13
1528.7–3117	95.9± 13.8	0.181± 0.026	0.29± 0.13	0.27± 0.17	$7.89^{+0.50}_{-0.60}$	$30.82^{+0.07}_{-0.29}$	S	6
1529.4–2850	125.8± 15.2	0.228± 0.028	0.39± 0.11	−0.17± 0.15	$6.78^{+0.10}_{-0.05}$	$30.73^{+0.08}_{-0.06}$	S	20
1530.4–3218	368.3± 24.6	0.718± 0.048	0.42± 0.06	0.08± 0.08	$7.04^{+0.05}_{-0.05}$	$31.25^{+0.03}_{-0.03}$	S	4
1530.8–3021	14.1± 5.9	0.026± 0.011	$0.91^{+0.09}_{-0.41}$	0.05± 0.43	$7.01^{+1.40}_{-0.35}$	$29.97^{+0.25}_{-0.30}$	S	24
1531.3–3329	47.2± 10.0	0.092± 0.020	0.09± 0.21	−0.36± 0.29	$6.55^{+0.05}_{-0.05}$	$30.37^{+0.44}_{-0.15}$	S	13
1531.5–3021	13.2± 5.9	0.022± 0.010	$0.93^{+0.07}_{-0.31}$	0.05± 0.43	$7.01^{+1.40}_{-0.35}$	$29.91^{+0.24}_{-0.30}$	S	17
1534.3–3300	25.5± 8.0	0.046± 0.014	0.11± 0.31	0.18± 0.38	$7.94^{+0.45}_{-0.80}$	$30.15^{+0.16}_{-0.21}$	S	6
1535.2–2828	27.7± 8.7	0.048± 0.015	0.25± 0.29	−0.73± 0.36	$6.36^{+0.05}_{-0.05}$	$30.56^{+0.25}_{-0.45}$	S	24
1535.8–2958	19.7± 7.9	0.034± 0.014	0.42± 0.36	0.56± 0.35	$7.42^{+1.00}_{-0.30}$	$30.33^{+0.16}_{-0.30}$	S	6
1536.5–3246	14.3± 5.4	0.025± 0.009	$1.00^{+0.00}_{-0.13}$	0.51± 0.33	$7.26^{+0.35}_{-0.15}$	$30.16^{+0.16}_{-0.24}$	S	22
1537.0–3136	1406.4± 38.2	0.373± 0.010	0.30± 0.03	0.05± 0.03	$7.06^{+0.05}_{-0.05}$	$30.97^{+0.01}_{-0.01}$	S/P	4
1537.8–3045	136.6± 16.8	0.045± 0.006	0.23± 0.12	−0.04± 0.14	$7.07^{+0.05}_{-0.35}$	$30.05^{+0.06}_{-0.08}$	S/P	15
1538.2–3229	46.1± 12.9	0.015± 0.004	$0.96^{+0.04}_{-0.26}$	0.36± 0.18	$7.16^{+1.25}_{-0.05}$	$29.79^{+0.18}_{-0.16}$	P	16
1538.9–3116	66.7± 10.1	0.018± 0.003	0.15± 0.18	0.23± 0.19	$7.88^{+0.50}_{-0.60}$	$29.77^{+0.10}_{-0.20}$	P	13
1539.0–2956	50.5± 8.1	0.013± 0.002	$0.93^{+0.07}_{-0.10}$	0.45± 0.15	$7.55^{+0.85}_{-0.40}$	$29.93^{+0.08}_{-0.18}$	P	5
1539.4–2958	61.9± 8.7	0.016± 0.002	0.58± 0.13	0.13± 0.15	$7.02^{+0.05}_{-0.05}$	$29.95^{+0.07}_{-0.06}$	S/P	19
1539.4–3446	43.1± 9.9	0.073± 0.017	0.68± 0.16	0.40± 0.25	$7.14^{+1.25}_{-0.10}$	$30.70^{+0.15}_{-0.13}$	S	10
1539.5–2953	21.0± 6.0	0.006± 0.002	−0.29± 0.24	0.31± 0.34	$7.71^{+0.70}_{-0.40}$	$29.20^{+0.14}_{-0.18}$	P	11
1540.2–3018	21.8± 5.9	0.010± 0.003	0.21± 0.31	−0.46± 0.28	$6.36^{+0.05}_{-0.05}$	$29.88^{+0.25}_{-0.28}$	P	30
1540.7–3121	43.2± 11.6	0.014± 0.004	−0.01± 0.26	0.56± 0.38	$7.37^{+1.05}_{-0.15}$	$29.54^{+0.17}_{-0.15}$	S/P	10
1540.9–3024	81.3± 11.2	0.023± 0.003	0.44± 0.14	0.14± 0.15	$7.06^{+0.05}_{-0.05}$	$29.77^{+0.25}_{-0.06}$	S/P	21
1541.9–3019	79.3± 13.0	0.025± 0.004	0.41± 0.14	0.04± 0.16	$7.03^{+0.05}_{-0.05}$	$29.79^{+0.08}_{-0.08}$	P	2
1543.4–2925	13.4± 5.5	0.022± 0.009	$1.00^{+0.00}_{-0.17}$	0.87± 0.45	$7.33^{+1.05}_{-0.25}$	$30.19^{+0.16}_{-0.26}$	S	23
1543.8–3306	94.8± 13.6	0.163± 0.023	0.20± 0.14	0.13± 0.19	$7.91^{+0.50}_{-0.55}$	$30.74^{+0.08}_{-0.22}$	S	11
1544.0–3311	43.0± 9.6	0.074± 0.017	0.55± 0.22	0.30± 0.24	$7.89^{+0.50}_{-0.75}$	$30.53^{+0.11}_{-0.55}$	S	12
1544.2–3117	19.6± 5.7	0.005± 0.002	$0.77^{+0.23}_{-0.26}$	−0.16± 0.24	$6.84^{+0.15}_{-0.30}$	$29.31^{+0.23}_{-0.24}$	P	16
1545.2–3417	79.1± 13.0	0.116± 0.019	$1.00^{+0.00}_{-0.02}$	0.89± 0.09	$7.39^{+1.00}_{-0.10}$	$31.04^{+0.08}_{-0.09}$	S	15
1545.5–3249	< 13.3	< 0.030	···	···	···	< 30.00	S	39
1545.6–3208	< 10.5	< 0.023	···	···	···	< 29.89	S	53
1545.8–3020	3028.9± 55.8	0.801± 0.015	−0.09± 0.02	0.04± 0.03	$7.85^{+0.05}_{-0.05}$	$31.33^{+0.01}_{-0.01}$	S/P	6
1546.0–2920	< 13.1	< 0.028	···	···	···	< 29.97	S	36
1546.1–2804	39.6± 9.6	0.063± 0.015	0.41± 0.23	0.05± 0.31	$7.04^{+0.05}_{-0.25}$	$30.45^{+0.13}_{-0.25}$	S	6
1546.7–3210	54.7± 8.2	0.012± 0.002	0.44± 0.15	−0.28± 0.17	$6.55^{+0.05}_{-0.05}$	$29.65^{+0.32}_{-0.33}$	P	10
1548.0–2908	36.4± 9.1	0.059± 0.015	0.57± 0.20	0.41± 0.23	$7.61^{+0.80}_{-0.40}$	$30.45^{+0.13}_{-0.25}$	S	2
1548.9–3045	44.8± 7.7	0.011± 0.002	0.83± 0.14	0.23± 0.17	$7.06^{+0.05}_{-0.05}$	$29.82^{+0.08}_{-0.09}$	P	9
1549.0–3102	652.6± 26.0	0.155± 0.006	0.40± 0.04	0.15± 0.05	$7.07^{+0.05}_{-0.05}$	$30.59^{+0.04}_{-0.02}$	S/P	3
1549.3–2600	56.5± 11.1	0.084± 0.017	$1.00^{+0.00}_{-0.02}$	0.14± 0.19	$7.03^{+0.05}_{-0.10}$	$30.68^{+0.09}_{-0.11}$	S	2
1550.0–2312	< 11.1	< 0.024	···	···	···	< 29.91	S	13
1550.9–2534	23.2± 7.4	0.036± 0.012	$1.00^{+0.00}_{-0.09}$	0.13± 0.31	$7.03^{+0.10}_{-0.15}$	$30.17^{+0.13}_{-0.20}$	S	6
1551.1–2402	33.2± 8.0	0.054± 0.013	$0.90^{+0.10}_{-0.21}$	0.50± 0.21	$7.29^{+1.10}_{-0.15}$	$30.45^{+0.13}_{-0.17}$	S	6
1551.4–3131	9.5± 4.5	0.017± 0.008	$1.00^{+0.00}_{-0.17}$	0.49± 0.43	$7.23^{+1.15}_{-0.25}$	$29.98^{+0.19}_{-0.35}$	S	5
1551.9–2621	78.6± 12.5	0.122± 0.019	$1.00^{+0.00}_{-0.02}$	−0.03± 0.16	$6.97^{+0.05}_{-0.05}$	$30.71^{+0.07}_{-0.08}$	S	8

TABLE 2
(CONTINUED) RESULTS OF ROSAT OBSERVATIONS. S/P INDICATES IF A SOURCE HAS BEEN DETECTED IN THE RASS ("S") OR IN POINTED OBSERVATIONS ("P").

RX J	counts	count rate [s^{-1}]	HR 1	HR 2	log T_X [K]	log L_X [erg/s]	S/P	sep. ["]
1552.5–3224	29.9± 8.7	0.053± 0.015	$0.84\pm^{+0.16}_{-0.18}$	−0.10± 0.29	$6.91^{+0.15}_{-0.30}$	$30.29^{+0.20}_{-0.18}$	S	13
1552.5–2633	11.8± 4.6	0.020± 0.008	0.59± 0.36	0.59± 0.39	$7.40^{+1.00}_{-0.30}$	$30.06^{+0.16}_{-0.30}$	S	4
1554.0–2920	23.8± 8.1	0.046± 0.016	0.50± 0.33	−0.19± 0.39	$6.56^{+0.40}_{-0.10}$	$30.27^{+0.33}_{-0.80}$	S	22
1554.9–2347	3750.7± 61.5	0.745± 0.012	0.27± 0.02	0.12± 0.02	$7.09^{+0.05}_{-0.05}$	$31.27^{+0.01}_{-0.01}$	S/P	3
1555.1–2521	303.6± 18.4	0.036± 0.002	0.92± 0.04	0.17± 0.06	$7.07^{+0.05}_{-0.05}$	$30.14^{+0.03}_{-0.03}$	S/P	9
1555.4–3338	19.9± 7.5	0.032± 0.012	0.38± 0.37	−0.03± 0.43	$7.02^{+0.15}_{-0.35}$	$29.90^{+0.27}_{-0.22}$	S	6
1555.6–3159	12.4± 5.7	0.020± 0.009	−0.19± 0.21	−0.25± 0.48	$6.15^{+0.05}_{-0.05}$	$29.83^{+1.72}_{-0.68}$	S	18
1555.8–2512	423.1± 22.0	0.053± 0.003	0.91± 0.03	0.06± 0.05	$7.02^{+0.05}_{-0.05}$	$30.30^{+0.04}_{-0.03}$	S/P	7
1557.3–2529	93.7± 22.9	0.014± 0.003	1.00± 0.00	0.53± 0.00	$7.32^{+0.05}_{-0.05}$	$29.99^{+0.09}_{-0.10}$	P	10
1557.8–2305	29.1± 7.4	0.052± 0.013	$0.95\pm^{+0.05}_{-0.15}$	0.70± 0.23	$7.30^{+1.10}_{-0.10}$	$30.46^{+0.13}_{-0.15}$	S	21
1558.1–2405	56.9± 20.2	0.008± 0.003	1.00± 0.00	0.52± 0.15	$7.15^{+0.05}_{-0.05}$	$29.66^{+0.14}_{-0.21}$	P	8
1558.2–2328	317.5± 23.7	0.101± 0.008	$1.00\pm^{+0.00}_{-0.03}$	−0.14± 0.22	$6.90^{+0.10}_{-0.15}$	$30.68^{+0.07}_{-0.05}$	S/P	7
1558.8–2512	86.0± 12.9	0.010± 0.001	0.76± 0.13	−0.01± 0.15	$6.93^{+0.05}_{-0.15}$	$29.79^{+0.05}_{-0.08}$	P	21
1559.2–2606	12.7± 5.6	0.021± 0.009	$1.00\pm^{+0.00}_{-0.17}$	0.59± 0.45	$7.27^{+1.15}_{-0.20}$	$30.07^{+0.18}_{-0.30}$	S	24
1559.6–3255	22.4± 6.8	0.041± 0.012	$1.00\pm^{+0.00}_{-0.04}$	0.35± 0.33	$7.12^{+1.30}_{-0.10}$	$30.39^{+0.18}_{-0.16}$	S	34
1559.8–2556	15.3± 5.6	0.028± 0.010	$1.00\pm^{+0.00}_{-0.12}$	0.15± 0.36	$7.02^{+0.10}_{-0.15}$	$30.01^{+0.15}_{-0.20}$	S	7
1600.0–2509	286.5± 21.3	0.034± 0.003	0.89± 0.05	0.28± 0.07	$7.12^{+0.05}_{-0.05}$	$30.14^{+0.05}_{-0.04}$	S/P	11
1600.2–2417	30.9±	0.007±	1.00± 0.00	0.38± 0.25	$6.45^{+0.15}_{-0.05}$	< 29.38	P	11
1600.5–2027	37.4± 9.6	0.066± 0.017	$1.00\pm^{+0.00}_{-0.06}$	0.46± 0.20	$7.20^{+1.20}_{-0.10}$	$30.63^{+0.14}_{-0.15}$	S	4
1600.6–2159	19.3± 7.0	0.031± 0.011	$1.00\pm^{+0.00}_{-0.12}$	0.75± 0.26	$7.32^{+1.10}_{-0.15}$	$30.30^{+0.15}_{-0.20}$	S	39
1600.7–2127	19.8± 6.9	0.037± 0.013	$1.00\pm^{+0.00}_{-0.11}$	−0.02± 0.35	$6.97^{+0.10}_{-0.15}$	$30.12^{+0.14}_{-0.20}$	S	11
1600.7–2343	< 18.9	< 0.048	...	...	...	< 30.21	S	0
1601.1–2113	22.2± 7.3	0.040± 0.013	$1.00\pm^{+0.00}_{-0.12}$	0.23± 0.31	$7.06^{+0.10}_{-0.10}$	$30.19^{+0.15}_{-0.19}$	S	25
1601.3–2652	47.7± 10.1	0.075± 0.016	$1.00\pm^{+0.00}_{-0.03}$	0.27± 0.20	$7.08^{+0.05}_{-0.10}$	$30.57^{+0.09}_{-0.13}$	S	10
1601.4–2240	35.9± 8.5	0.068± 0.016	$1.00\pm^{+0.00}_{-0.05}$	0.09± 0.24	$7.00^{+0.10}_{-0.15}$	$30.58^{+0.10}_{-0.13}$	S	10
1601.7–2049	26.9± 7.9	0.050± 0.015	$1.00\pm^{+0.00}_{-0.07}$	−0.17± 0.29	$6.84^{+0.15}_{-0.25}$	$30.40^{+0.18}_{-0.17}$	S	11
1601.8–2445	206.8± 26.0	0.031± 0.004	$1.00\pm^{+0.00}_{-0.09}$	0.45± 0.34	$7.19^{+1.20}_{-0.15}$	$30.28^{+0.12}_{-0.12}$	S/P	8
1601.9–2008	78.9± 12.7	0.141± 0.023	$1.00\pm^{+0.00}_{-0.02}$	0.35± 0.15	$7.11^{+0.10}_{-0.05}$	$30.97^{+0.07}_{-0.08}$	S	2
1602.0–2221	22.8± 7.4	0.040± 0.013	0.51± 0.28	0.51± 0.26	$7.88^{+0.50}_{-0.80}$	$30.54^{+0.12}_{-0.28}$	S	15
1602.1–2241	36.7± 8.4	0.064± 0.015	$0.97\pm^{+0.03}_{-0.13}$	0.53± 0.19	$7.30^{+1.10}_{-0.15}$	$30.57^{+0.12}_{-0.16}$	S	6
1602.8–2401	< 13.6	< 0.032	...	...	...	< 30.03	S	19
1602.9–2022	58.8± 11.4	0.105± 0.020	0.87± 0.11	0.34± 0.18	$7.10^{+0.10}_{-0.05}$	$30.87^{+0.08}_{-0.10}$	S	24
1603.6–2245	113.1± 13.9	0.206± 0.025	0.93± 0.06	0.28± 0.12	$7.11^{+0.05}_{-0.05}$	$31.02^{+0.06}_{-0.06}$	S	7
1603.9–2031	46.4± 9.1	0.087± 0.017	$1.00\pm^{+0.00}_{-0.02}$	0.32± 0.18	$7.09^{+0.05}_{-0.05}$	$30.81^{+0.08}_{-0.11}$	S	13
1604.3–2130	29.4± 7.5	0.054± 0.014	$0.95\pm^{+0.05}_{-0.21}$	0.39± 0.26	$7.12^{+1.30}_{-0.05}$	$30.58^{+0.17}_{-0.13}$	S	7
1604.7–1930	21.9± 6.2	0.041± 0.012	$0.91\pm^{+0.09}_{-0.15}$	0.66± 0.24	$7.33^{+1.05}_{-0.20}$	$30.43^{+0.14}_{-0.17}$	S	16
1605.6–2152	20.2± 6.8	0.033± 0.011	$1.00\pm^{+0.00}_{-0.12}$	−0.38± 0.34	$6.56^{+0.35}_{-0.20}$	$30.49^{+0.47}_{-0.61}$	S	4
1605.7–2004	11.2± 5.3	0.019± 0.009	$1.00\pm^{+0.00}_{-0.18}$	0.45± 0.44	$7.16^{+1.25}_{-0.20}$	$30.14^{+0.20}_{-0.29}$	S	13
1606.2–2036	30.9± 8.4	0.050± 0.014	$1.00\pm^{+0.00}_{-0.06}$	−0.20± 0.27	$6.71^{+0.25}_{-0.25}$	$30.69^{+0.35}_{-0.25}$	S	2
1606.3–1928	16.0± 5.7	0.030± 0.011	$1.00\pm^{+0.00}_{-0.12}$	0.17± 0.38	$7.05^{+1.35}_{-0.25}$	$30.18^{+0.21}_{-0.22}$	S	8
1606.6–2108	9.6± 4.2	0.016± 0.007	$1.00\pm^{+0.00}_{-0.20}$	0.38± 0.19	$7.12^{+1.30}_{-0.05}$	$30.02^{+0.19}_{-0.26}$	S	3
1607.0–2043	27.5± 8.0	0.044± 0.013	$0.91\pm^{+0.09}_{-0.14}$	0.08± 0.29	$6.99^{+0.10}_{-0.30}$	$30.41^{+0.14}_{-0.16}$	S	19
1607.0–2036	38.8± 9.0	0.060± 0.014	$1.00\pm^{+0.00}_{-0.03}$	0.69± 0.17	$7.25^{+0.20}_{-0.05}$	$30.54^{+0.10}_{-0.13}$	S	4
1607.0–1911	62.4± 10.8	0.099± 0.017	$0.97\pm^{+0.03}_{-0.11}$	0.79± 0.12	$7.38^{+1.00}_{-0.15}$	$30.94^{+0.10}_{-0.09}$	S	9

TABLE 3
JOURNAL OF GROUND-BASED FOLLOW-UP OBSERVATIONS.

Date	Telescope	Instrument	spectral range/filter
1992 Mar 27 to Jun 1	ESO 1.52m	B&C	520 nm – 780 nm
1992 Jun 1 to 3	ESO/MPI 2.2m	EFOSC2	520 nm – 780 nm
1993 Jun 13 to 19	ESO 1.52m	B&C	520 nm – 780 nm
1993 Jun 22 to 29	Dutch 90cm	CCD	BVRI
1993 Jul 3 to 9	ESO 1.0m	IR Phot	JHKL
1994 May 15 to 21	ESO 1.52m	B&C	520 nm – 780 nm
1994 May 21 to 25	ESO 1.0m	IR Phot	JHKL
1995 Apr 16 ro 19	Danish 1.54m	CCD	BVRI
1995 Jun 13 to 16	Danish 1.54m	CORAVEL	optical
1996 May 31 to Jun 4	Danish 1.54m	CORAVEL	optical

TABLE 4
PHOTOMETRY OF X-RAY ACTIVE STARS IN UPPER SCORPIUS

RX J	V [mag]	B–V [mag]	V–R [mag]	R–I [mag]	J [mag]	J–H [mag]	H–K [mag]	K–L [mag]
1524.2–3030A	10.89	0.86	0.50	0.49	9.47	0.42	0.09	−0.05†
1524.2–3030B	13.58	1.42	0.98	1.08	...	...	...	...
1528.7–3117	8.95	0.79	0.46	0.44	7.52	0.49	0.11	0.07
1529.4–2850A	8.67*	0.71*	0.44*	0.41*	...	...	...	...
1529.4–2850B	8.67*	0.71*	0.44*	0.41*	...	...	...	...
1530.4–3218	8.85	0.71	0.43	0.39	7.46	0.38	0.12	0.05
1530.8–3021	11.36	1.03	0.58	0.53	9.42	0.57	0.16	...
1531.3–3329	10.89	0.82	0.49	0.45	9.43	0.45	0.14	0.31†
1531.5–3021	13.17	1.33	0.93	0.97	10.24	0.73	0.42†	...
1534.3–3300	12.63	1.29	0.85	0.78	10.11	0.75	0.20	...
1535.2–2828	8.11	0.65	0.33	0.17†	...	...	...	...
1535.8–2958	14.93	1.38	1.38	1.67	10.39	0.59	0.31	...
1536.5–3246	14.73	1.51	1.27	1.58	10.58	0.62	0.30	...
1537.0–3136A	10.02	0.78	0.46	0.47	7.87*	0.55*	0.19*	0.12*
1537.0–3136B	11.88	1.26	0.97	1.09	7.87*	0.55*	0.19*	0.12*
1537.8–3045	11.37	1.01	0.62	0.60	9.35	0.57	0.17	0.31†
1538.2–3229	10.52	0.69	0.41	0.37	...	...	...	...
1538.9–3116	14.93	1.30	1.17	1.49	10.70	0.61	0.28	...
1539.0–2956	13.09	1.30	0.78	0.77	...	...	...	...
1539.4–2958	15.16	1.58	1.18	1.40	...	...	...	...
1539.4–3446A	9.45	0.59	0.39	0.57	7.80	0.31	0.04	0.05
1539.4–3446B	12.18	1.45	0.94	0.95	8.87*	0.77*	0.35*	0.57*
1539.4–3446C	15.27	1.52	1.37	1.55	8.87*	0.77*	0.35*	0.57*
1539.5–2953	15.80	1.48	1.28	1.55	11.56	0.56	0.31	...
1540.2–3018	16.53†	1.17†	1.19†	1.44†	...	...	...	...
1540.7–3121A	15.06	1.44	1.28	1.53	10.77*	0.64*	0.24*	...
1540.7–3121B	15.09	1.56	1.27	1.56	10.77*	0.64*	0.24*	...
1540.9–3024	14.53	1.40	1.13	1.34	10.70	0.68	0.23	...
1541.9–3019	16.06	1.32	1.27	1.53	...	...	...	...
1543.4–2925	11.36	1.05	0.63	0.61	9.27	0.59	0.15	0.09
1543.8–3306	14.86	1.38	1.27	1.59	10.66	0.62	-0.19†	
1544.0–3311	10.83	0.88	0.53	0.52	9.05	0.53	0.15	0.13
1544.2–3117	12.28	0.79	0.45	0.44	...	...	...	...
1545.2–3417	10.22	1.22	0.78	0.70	7.66	0.73	0.21	...
1545.5–3249	12.85	1.19	0.66	0.62	...	...	...	...
1545.6–3208	11.21	1.50	0.84	0.80	8.51	0.76	0.24	0.22
1545.8–3020	9.33	0.98	0.63	0.63	7.31	0.61	0.16	0.10
1546.0–2920	13.46	1.44	0.94	0.95	...	...	...	...
1546.1–2804	9.27	0.77	0.45	0.39	7.96	0.45	0.08	0.07
1546.7–3210	14.81	1.50	1.08	1.24	...	...	...	...
1548.0–2908	11.15	0.90	0.47	0.38	9.32	0.46	0.14	0.16
1548.9–3045	15.28	1.56	1.23	1.40	...	...	...	...
1549.0–3102	11.01	0.85	0.50	0.54	9.27	0.51	0.14	0.15
1549.3–2600	11.02	1.11	0.67	0.64	8.80	0.65	0.16	0.18
1550.0–2312	16.08	1.38	0.83†	0.71†	...	...	...	...
1550.9–2534	9.62	0.64	0.39	0.36	...	...	...	...
1551.1–2402	14.35	1.59	1.08	1.19	...	...	...	...
1551.4–3131	13.54	1.46	1.04	1.22	10.19	0.82	...	...
1551.9–2621	9.50	0.63	0.39	0.35	...	...	...	...

NOTE.— *: unresolved binary or multiple system; †: photometric uncertainty >0.1 mag

TABLE 4
PHOTOMETRY OF X-RAY ACTIVE STARS IN UPPER SCORPIUS

RX J	V [mag]	B–V [mag]	V–R [mag]	R–I [mag]	J [mag]	J–H [mag]	H–K [mag]	K–L [mag]
1552.5–2633	12.40	1.23	0.77	0.75	10.14	0.69	0.34	...
1552.5–3224A	14.88*	1.43*	1.13*	1.32*	11.91	0.71	0.34	...
1552.5–3224B	14.88*	1.43*	1.13*	1.32*	11.97	0.69	0.28	...
1554.0–2920	12.41	1.33	0.87	0.91	9.63	0.71	0.19	0.26†
1554.9–2347	8.93	0.65	0.41	0.40	7.57	0.39	0.07	...
1555.1–2521	12.32	1.43	0.89	0.86	9.68	0.78	0.38	...
1555.4–3338	12.36	1.13	0.69	0.67	10.19	0.66	0.16	...
1555.6–3159	13.77	1.54	1.28	1.59	9.58	0.58	0.31	...
1555.8–2512	10.32	0.78	0.46	0.42	...	...	...	...
1557.3–2529	12.68	1.33	0.89	0.85	9.76	0.71	0.19	...
1557.8–2305	13.36	1.53	0.95	0.95	10.22	0.75	0.21	...
1558.1–2405A	12.20	1.06	0.71	0.67	...	...	...	...
1558.1–2405B	16.76	1.82	1.39	1.66†	...	...	...	...
1558.2–2328	10.24	0.78	0.52	0.47	8.62	0.44	0.13	0.08
1558.8–2512	14.10	1.53	1.07	1.14	10.62	0.74	0.24	...
1559.2–2606	12.32	1.02	0.67	0.74	9.93	0.64	0.19	0.09
1559.6–3255	12.18	1.16	0.61	0.57	...	...	...	...
1559.8–2556	14.21	1.19	1.01	1.31	10.60	0.72	0.27	...
1600.0–2509	10.41	0.57	0.36	0.36	9.25	0.33	0.08	...
1600.2–2417	13.66	1.44	0.94	1.04	...	...	...	...
1600.5–2027	13.52	1.59	1.06	1.22	9.96	0.83	0.23	0.16
1600.6–2159	11.11	1.01	0.60	0.56	9.61	0.54	0.24	0.12
1600.7–2127	12.67	1.26	0.82	0.88	10.05	0.76	0.22	...
1600.7–2343	15.64	1.36	1.42	1.52	11.39†	0.61†	0.48†	...
1601.1–2113	12.54	1.30	0.82	0.86	9.77	0.74	0.21	0.23†
1601.3–2652	9.39	0.62	0.40	0.39	8.11	0.42	0.12	-0.04†
1601.4–2240	11.37	0.99	0.65	0.62	9.26	0.62	0.16	0.18
1601.7–2049	12.98	1.46	0.98	1.08	9.56	0.74	0.24	0.11†
1601.8–2445	12.28	1.35	0.90	0.84	9.44	0.73	0.20	...
1601.9–2008	10.45	0.96	0.58	0.58	8.50	0.56	0.17	0.04
1602.0–2221	13.55	1.58	1.09	1.23	9.94	0.75	0.27	0.12†
1602.1–2241	11.22	1.15	0.70	0.72	8.98	0.68	0.20	0.18
1602.8–2401A	11.05	1.26	0.75	0.67	10.02*	0.69*	0.34*	0.19*
1602.8–2401B	12.29	1.20	0.76	0.71	10.02*	0.69*	0.34*	0.19*
1602.9–2022	12.49	1.46	0.95	0.96	9.28	0.75	0.26	0.25
1603.6–2245	10.98	1.03	0.58	0.46	9.10	0.53	0.15	0.05
1603.9–2031A	12.84	1.07	1.11	0.81	9.77	0.81	0.40	...
1603.9–2031B	13.49	1.26	1.29	1.10	9.73	0.79	0.26	0.16†
1604.3–2130A	12.16	1.17	0.79	0.73	10.11†	0.91†	0.6 1†	...
1604.3–2130B	15.06	1.59	1.36	1.57	10.54†	0.72†	0.3 2†	0.01†
1604.7–1930	11.17	1.12	0.70	0.66	8.92	0.62	0.18	...
1605.6–2152	14.26	1.53	1.15	1.18	...	...	...	...
1605.7–2004	14.25	1.61	1.19	1.38	10.23	0.77	0.27	0.22
1606.2–2036	13.21	1.50	0.94	1.00	9.96	0.76	0.25	...
1606.3–1928	13.38	1.45	0.98	1.09	9.87	0.81	0.35	0.29
1606.6–2108	14.20	1.56	1.20	1.33	10.15	0.80	0.26	0.13
1607.0–2043	14.51	1.53	1.14	1.22	...	...	...	...
1607.0–2036	12.01	1.40	0.89	0.90	9.37†	0.63†	0.66†	0.17†
1607.0–1911	14.16	1.62	1.12	1.23	10.30	0.76	0.27	...

NOTE.—(continued); *: unresolved binary or multiple system; †: photometric uncertainty >0.1 mag

TABLE 5
RADIAL VELOCITIES AND V SIN I VALUES

Target name	v_{rad} [km s^{-1}]	v sin i [km s^{-1}]	remark
RXJ1524.2-3030A	0.66±0.27	11.8±1.1	
RXJ1528.7-3117	127.28±0.45	14.4±0.5	SB
RXJ1529.4-2850A	-12.10±0.42	6.1±0.9	SB
RXJ1530.4-3218	-2.33±1.12	49.0±6.6	SB
RXJ1530.8-3021	-0.33±0.43	21.5±2.1	
RXJ1531.3-3329	-1.86±0.34	15.3±1.0	
RXJ1531.5-3021	0.09±0.60	12.4±2.0	SB
RXJ1534.3-3300	0.92±0.39	9.2±1.6	
RXJ1535.2-2828	30.56±0.14	5.4±0.7	
RXJ1537.0-3136A	0.48±1.12	31.2±4.3	
RXJ1537.0-3136B	14.54±2.33	2.8±8.7	
RXJ1537.8-3045	0.26±0.25	14.8±1.0	
RXJ1538.2-3229	-8.11±6.86	35.8	
RXJ1539.4-3446A	-4.14±0.19	4.5±1.1	
RXJ1539.4-3446B	-1.78±0.71	21.0±3.9	
RXJ1543.4-2925	29.54±0.46	7.8±0.8	SB
RXJ1544.0-3311	-1.30±0.28	10.2±1.3	
RXJ1545.2-3417	-5.22±1.24	50.3±12.5	
RXJ1545.6-3208	-92.85±0.22	4.0±2.1	
RXJ1545.8-3020	-5.86±0.27	10.2±0.8	
RXJ1546.1-2804	-22.38±0.55	6.4±0.9	
RXJ1548.0-2908	-2.12±0.85	35.6±3.6	
RXJ1549.3-2600	-6.46±0.85	32.3±3.2	
RXJ1550.9-2534	-5.59±2.08	45.8±13.3	SB
RXJ1551.9-2621	-6.13±0.91	53.5±12.7	

TABLE 5
RADIAL VELOCITIES AND V SIN I VALUES

Target name	v_{rad} [km s^{-1}]	v sin i [km s^{-1}]	remark
RXJ1552.5-2633	-2.98±0.77	15.8±1.5	
RXJ1554.0-2920	-9.23±0.69	8.7	
RXJ1554.9-2347	-4.84±1.30, -9:[1]	57[1]	
RXJ1555.1-2521	-5.27±0.68	10.9±3.1	
NTTS155219-2314	-5:[1]	...	
RXJ1555.4-3338	-0.17±0.33	5.7±2.9	
RXJ1555.8-2512	-1.49±0.35	16.3±1.2	
NTTS155331-2340	-3.9	<12	
RXJ1557.3-2529	-4.79±1.87	9.2	
NTTS155421-2330	-1.6[1]	18[1]	
NTTS155427-2346	-5.1[1]	...	
NTTS155436-2313	-3.5[1]	35[1]	
RXJ1557.8-2305	-3.95±0.68	8.2±4.0	
RXJ1558.1-2405A	-3.41±4.66	4.0	
RXJ1558.2-2328	-5.97±0.70	23.4±3.6	
NTTS155703-2212	...	40[1]	
RXJ1600.0-2509	-4.33±0.92	28.4±2.8	
RXJ1600.6-2159	-3.64±0.85	35.7±3.6	
RXJ1600.7-2127	-3.74±1.67	10.2	
NTTS155808-2219	-4.9[1]	27[1]	SB
RXJ1601.4-2240	-6.82±0.59, -6.3[1]	10.0±1.5, 10[1]	
RXJ1601.7-2049	-7.66±1.50	11.1±6.2	
RXJ1601.8-2445	-5.81±1.03	11.8±4.8	
RXJ1601.9-2008	-4.46±1.54	72.2±18.9	
NTTS155910-2247	-4.9[1]	...	
RXJ1602.1-2241	0.93±1.00, -2.3[1]	24.6±4.6	SB
RXJ1602.8-2401A	105.50±0.28	1.1	
RXJ1603.6-2245	-8.83±0.95	35.9±10.0	
RXJ1603.9-2031B	-4.23±0.79	7.5±	
RXJ1603.9-2031A	-6.54±0.65	9.1±3.5	
RXJ1604.3-2130A	-6.22±0.63	12.4±2.7	
RXJ1604.7-1930	-3.12±1.94	67.1±13.5, 45[1]	
NTTS160233-1931	-3.6[1]	...	
RXJ1605.7-2004	-6.3[1]	<12[1]	
RXJ1606.2-2036	-5.30±0.56	5.9±4.3	
RXJ1606.3-1928	-3.7[1]	<15[1]	
NTTS160345-1953	-3.0[1]	...	
NTTS160728-1856	-7.0[1]	...	
NTTS160735-1857	-7.3[1]	...	
NTTS160814-1857	-6.6[1]	22[1]	SB
NTTS160827-1813	-7.7[1]	14[1]	
NTTS160905-1859	-6.4[1]	21[1]	SB
NTTS160946-1851	-5:[1]	77[1]	
NTTS161431-2256	-3.3[1]	35[1]	

NOTE.—SB: Spectroscopic Binary

REFERENCES.—[1] Walter et al. (1994)

TABLE 6
PHYSICAL PARAMETERS OF TARGET STARS

Target name	W(Hα) [Å]	W(Li) [Å]	SpT	log T_{eff} [K]	TTS class	A_V [mag]	log L_X/L_{bol}	log L_{bol} [$L_\odot$]
RXJ1524.2-3030A	1.64	0.41	K0	3.721	WTTS	0.24	-3.21	0.026
RXJ1524.2-3030B	-3.23	0.38	M0	3.561	PTTS	0.20	···	-0.589
RXJ1528.0-2600	-1.66	0.10	K3	3.675	????	0.54	-3.30	-0.121
RXJ1528.7-3117	1.68	0.13	G8	3.743	????	0.25	-3.55	0.769
RXJ1529.4-2850A	2.43	0.13	G8	3.743	????	0.15	-3.73	0.842
RXJ1530.4-3218	1.84	0.34	G7	3.751	????	0.15	-3.12	0.761
RXJ1530.8-3021	1.07	0.46	K2	3.691	WTTS	0.21	-3.55	-0.115
RXJ1531.3-3329	1.33	0.44	G8	3.743	????	0.32	-3.23	0.024
RXJ1531.5-3021	-2.93	0.35	M0	3.575	PTTS	0.17	-3.25	-0.504
RXJ1534.3-3300	-0.60	0.41	M0	3.575	PTTS	0.00	-3.18	-0.358
RXJ1535.2-2828	3.13	0.15	G0	3.778	????	0.00	-4.14	0.973
RXJ1535.8-2958	-25.62	0.59	M4	3.502	CTTS	0.34	-2.80	-0.591
RXJ1536.5-3246	-6.21	0.09	M3	3.526	PTTS	0.77	-2.82	-0.569
RXJ1537.0-3136A	1.34	0.45	G7	3.751	????	0.37	-3.01	0.378
RXJ1537.0-3136B	-3.67	0.38	K7	3.612	PTTS	1.14	···	0.247
RXJ1537.8-3045	-1.31	0.62	K4	3.658	WTTS	0.10	-3.53	-0.092
RXJ1538.2-3229	3.32	0.06	G3	3.768	????	0.20	-3.92	0.097
RXJ1538.9-3116	-7.31	0.14	M2	3.546	PTTS	0.97	-2.89	-0.721
RXJ1539.0-2956	-1.05	0.23	K4	3.658	????	0.74	-3.11	-0.525
RXJ1539.4-2958	-6.09	0.25	M2	3.546	PTTS	0.81	-2.83	-0.875
RXJ1539.4-3446A	4.13	0.19	G1	3.774	????	0.60	-3.65	0.677
RXJ1539.4-3446B	-6.59	0.70	K7	3.612	CTTS	0.81	···	-0.004
RXJ1539.4-3446C	-49.29	0.48	M2	3.546	CTTS	1.76	···	-0.539
RXJ1539.5-2953	-4.79	0.05	M3	3.526	PTTS	0.74	-3.35	-1.013
RXJ1540.2-3018	-4.21	0.07	M3	3.526	PTTS	0.35	-2.28	-1.460
RXJ1540.7-3121A	-4.08	0.12	M4	3.502	PTTS	0.00	-3.40	-0.781
RXJ1540.7-3121B	-4.98	0.06	M5	3.474	PTTS	0.00	···	-0.462
RXJ1540.9-3024	-5.48	0.11	M2	3.546	PTTS	0.60	-3.05	-0.708
RXJ1541.9-3019	-7.72	0.19	M4	3.502	PTTS	0.00	-2.70	-1.181
RXJ1543.4-2925	0.95	0.05	K0	3.721	????	0.72	-3.50	0.031
RXJ1543.8-3306	-8.11	0.04	M3	3.526	????	0.79	-2.15	-0.613
RXJ1544.0-3311	-0.82	0.33	G9	3.733	????	0.45	-3.12	0.116
RXJ1544.2-3117	1.92	0.19	G3	3.768	????	0.42	-3.80	-0.522
RXJ1545.2-3417	-6.38	0.51	K0	3.721	CTTS	1.19	-3.28	0.673
RXJ1545.5-3249	0.97	0.10	G9	3.733	????	0.90	<-3.15	-0.514
RXJ1545.6-3208	0.95	0.09	K3	3.675	????	1.09	<-4.14	0.328
RXJ1545.8-3020	-0.82	0.43	K3	3.675	PTTS	0.35	-3.04	0.786
RXJ1546.0-2920	-1.29	0.42	M0	3.575	PTTS	0.16	<-3.14	-0.628
RXJ1546.1-2804	2.30	0.16	G9	3.733	????	0.05	-3.82	0.577
RXJ1546.7-3210	-2.73	0.15	M2	3.546	PTTS	0.31	-3.25	-0.937
RXJ1548.0-2908	1.53	0.40	G9	3.733	????	0.07	-3.14	-0.167
RXJ1548.9-3045	-2.92	0.09	M2	3.546	PTTS	0.91	-2.94	-0.884
RXJ1549.0-3102	0.41	0.43	K0	3.721	WTTS	0.34	-3.02	0.016
RXJ1549.3-2600	1.14	0.38	K0	3.721	WTTS	0.86	-3.16	0.222
RXJ1550.0-2312	-3.79	0.04	M2	3.546	????	0.00	<-2.27	-1.568
RXJ1550.9-2534	3.60	0.09	G1	3.783	????	0.25	-3.93	0.469
RXJ1551.1-2402	-2.66	0.38	M2	3.546	PTTS	0.21	-2.45	-0.791
RXJ1551.4-3131	-2.33	0.33	M0	3.561	PTTS	0.58	-3.20	-0.418
RXJ1551.9-2621	3.01	0.19	G0	3.778	????	0.20	-3.43	0.496

TABLE 6
PHYSICAL PARAMETERS OF TARGET STARS(CONTINUED)

Target name	W(Hα) [Å]	W(Li) [Å]	SpT	log T_{eff} [K]	TTS class	A_V [mag]	log L_X/L_{bol}	log L_{bol} [$L_\odot$]
RXJ1552.5-3224A	-6.70	0.46	M2	3.546	PTTS	0.56	-2.43	-0.864
RXJ1552.5-2633	-2.45	0.47	M0	3.575	PTTS	0.00	-3.44	-0.266
RXJ1554.0-2920	-2.96	0.37	M0	3.575	PTTS	0.00	-3.20	-0.270
RXJ1554.9-2347	1.75	0.25	G2	3.771	????	0.28	-3.12	0.762
RXJ1555.1-2521	-1.05	0.46	M0	3.561	PTTS	0.00	-3.37	-0.164
NTTS155219-2314	-13.30	0.40:	M2	3.536	PTTS	0.00	···	-0.750
NTTS155220-2313	-4.60	···	M4	3.502	????	0.00	-3.60	-0.373
RXJ1555.4-3338	-1.31	0.35	K5	3.641	PTTS	0.19	-3.28	-0.414
RXJ1555.6-3159	-2.58	0.14	M2	3.546	PTTS	1.38	-3.50	-0.094
RXJ1555.8-2512	2.65	0.26	G3	3.768	????	0.40	-3.57	0.254
NTTS155331-2340	-1.45	0.10	M1	3.554	PTTS	0.08	-3.41	-0.365
NTTS155357-2321	-3.67	0.00	M3	3.526	????	0.35	-3.14	-1.028
RXJ1557.3-2529	-2.45	0.46	M0	3.575	PTTS	0.00	-3.42	-0.378
NTTS155421-2330	-0.71	0.28	M0	3.575	PTTS	0.04	-3.57	-0.403
NTTS155427-2346	-0.94	0.68	M0	3.568	WTTS	0.74	-3.20	-0.467
NTTS155436-2313	-4.25	0.58	M0	3.561	WTTS	0.58	-3.22	-0.454
RXJ1557.8-2305	-1.45	0.45	M0	3.575	PTTS	0.12	-2.69	-0.604
RXJ1558.1-2405B	-9.31	0.00	M5	3.474	????	0.00	···	-1.130
RXJ1558.1-2405A	-1.82	0.36	K4	3.658	PTTS	0.41	-3.63	-0.300
RXJ1558.2-2328	1.97	0.29	G2	3.771	????	0.63	-3.32	0.378
RXJ1558.8-2512	-2.11	0.09	M0	3.561	????	0.49	-3.35	-0.681
RXJ1559.2-2606	-0.53	0.26	K2	3.691	????	0.80	-3.18	-0.267
RXJ1559.6-3255	0.47	0.25	G8	3.743	????	1.17	-2.95	-0.151
RXJ1559.8-2556	-6.48	0.31	M2	3.546	PTTS	0.35	-2.85	-0.681
NTTS155703-2212	-4.45	0.49	M0	3.561	PTTS	0.41	-3.10	-0.372
RXJ1600.0-2509	3.15	0.21	G0	3.778	????	0.16	-3.61	0.117
RXJ1600.2-2417	-2.43	0.47	M0	3.575	PTTS	0.33	-3.71	-0.638
RXJ1600.5-2027	-4.01	0.48	M0	3.561	PTTS	0.62	-2.68	-0.395
RXJ1600.6-2159	1.37	0.50	G9	3.733	????	0.67	-3.42	0.089
RXJ1600.7-2127	-1.86	0.31	K7	3.612	PTTS	0.44	-3.03	-0.348
RXJ1600.7-2343	-8.05	0.02	M2	3.546	????	1.51	<-2.28	-0.788
NTTS155808-2219	-3.32	0.55	M3	3.526	WTTS	0.04	-3.50	-0.468
RXJ1601.1-2113	-2.72	0.42	M0	3.575	PTTS	0.00	-3.19	-0.322
RXJ1601.3-2652	3.01	0.14	G0	3.778	????	0.29	-3.67	0.579
RXJ1601.4-2240	-0.50	0.46	K1	3.707	WTTS	0.66	-3.06	0.029
RXJ1601.7-2049	-4.19	0.43	M0	3.575	PTTS	0.48	-2.99	-0.304
RXJ1601.8-2445	-1.35	0.44	K7	3.612	PTTS	0.52	-3.27	-0.161
RXJ1601.9-2008	0.97	0.40	G5	3.762	????	0.70	-3.09	0.328
RXJ1602.0-2221	-3.74	0.37	M0	3.561	PTTS	0.70	-2.84	-0.376
NTTS155910-2247	-0.22	0.45	M0	3.561	PTTS	0.43	-2.77	-0.700
RXJ1602.1-2241	-0.48	0.21	K4	3.658	????	0.49	-3.18	0.123
RXJ1602.8-2401B	-0.92	0.53	K4	3.658	WTTS	0.59	···	-0.267
RXJ1602.8-2401A	1.44	0.07	K0	3.721	????	1.07	<-3.95	0.295
RXJ1602.9-2022	-3.37	0.48	K7	3.612	PTTS	0.85	-2.74	-0.113
RXJ1603.6-2245	1.49	0.31	G9	3.733	????	0.44	-2.72	0.048
RXJ1603.9-2031B	-4.20	0.47	M0	3.575	PTTS	1.12	···	-0.253
RXJ1603.9-2031A	-25.17	0.49	K5	3.641	CTTS	1.27	-2.70	-0.172
RXJ1604.3-2130B	-6.45	0.38	M2	3.546	PTTS	1.49	···	-0.564
RXJ1604.3-2130A	-7.00	0.38	K2	3.691	CTTS	1.01	-2.96	-0.118
RXJ1604.7-1930	-0.17	0.32	K3	3.675	????	0.54	-3.38	0.127
NTTS160233-1931	-2.63	1.30	M0	3.561	WTTS	0.31	-2.52	-0.755
RXJ1605.6-2152	-5.36	0.50	M0	3.561	PTTS	0.72	-2.57	-0.652
RXJ1605.7-2004	-5.84	0.67	M0	3.561	WTTS	1.18	-3.02	-0.462
RXJ1606.2-2036	-2.84	0.58	K5	3.641	WTTS	1.31	-2.65	-0.305
RXJ1606.3-1928	-16.77	0.48	M0	3.575	CTTS	0.50	-3.04	-0.457
RXJ1606.6-2108	-4.08	0.49	M0	3.561	PTTS	1.11	-3.08	-0.473

TABLE 6
PHYSICAL PARAMETERS OF TARGET STARS (CONTINUED)

Target name	W(Hα) [Å]	W(Li) [Å]	SpT	log T_{eff} [K]	TTS class	A_V [mag]	log L_X/L_{bol}	log L_{bol} [$L_\odot$]
NTTS160345-1953	-4.23	0.70:	M3	3.526	WTTS	0.31	-2.85	-1.023
RXJ1607.0-2043	-3.22	0.55	M0	3.561	WTTS	0.78	-2.56	-0.729
RXJ1607.0-1911	-5.34	0.44	M0	3.561	PTTS	0.76	-2.28	-0.597
RXJ1607.0-2036	-2.70	0.62	M0	3.575	WTTS	0.00	-3.13	-0.110
NTTS160728-1856	-3.79	0.50	M0	3.561	PTTS	1.38	...	-0.657
NTTS160735-1857	-2.94	0.61	M3	3.526	WTTS	0.00	-3.14	-0.527
NTTS160814-1857	-0.71	0.45	K2	3.691	WTTS	1.49	-3.24	0.164
NTTS160827-1813	-0.01	0.43	K5	3.641	PTTS	0.88	-3.70	-0.170
NTTS160836-1843	-2.91	0.00	M4	3.502	????	0.19	-3.01	-0.957
NTTS160905-1859	0.27	0.37	K0	3.721	WTTS	1.21	-3.57	0.101
NTTS160927-1901	-4.17	2.10:	M2	3.536	WTTS	0.77	-2.76	-0.909
NTTS160946-1851	-0.35	0.38	K0	3.721	WTTS	1.09	-3.37	0.399
NTTS161431-2256	0.71	0.24	G0	3.778	????	0.60	-3.29	0.423

TABLE 7
TARGET LIST

Target name	α (2000)	δ (2000)	TTS class	Alias	remark
RXJ1524.2-3030A	15 24 11.5	-30 30 57	WTTS		
RXJ1524.2-3030B	15 24 13.0	-30 30 55	PTTS		
RXJ1528.0-2600	15 28 03.2	-26 00 02	????		
RXJ1528.7-3117	15 28 42.0	-31 17 39	????	HIP 75769	SB[7], VB[3,4,5]
RXJ1529.4-2850A	15 29 26.9	-28 50 51	????	HIP 75836	SB[7], VB[4], EB
RXJ1530.4-3218	15 30 26.2	-32 18 11	????	HIP 75924	SB[7], VB[3,4,5]
RXJ1530.8-3021	15 30 28.0	-30 20 53	WTTS		
RXJ1531.3-3329	15 31 21.9	-33 29 39	????		
RXJ1531.5-3021	15 31 29.6	-30 21 53	PTTS		SB[7], VT[4]
RXJ1534.3-3300	15 34 23.1	-33 00 07	PTTS		
RXJ1535.2-2828	15 35 13.5	-28 28 26	????	HIP 76304	
RXJ1535.8-2958	15 35 48.3	-29 58 54	CTTS		VB[3,4]
RXJ1536.5-3246	15 36 33.7	-32 46 10	PTTS		VB[3,4]
RXJ1537.0-3136A	15 37 02.0	-31 36 38	????		VB[3,4]
RXJ1537.0-3136B	15 37 02.0	-31 36 38	PTTS		VB[3]
RXJ1537.8-3045	15 37 51.3	-30 45 15	WTTS		
RXJ1538.2-3229	15 38 16.1	-32 29 22	????		
RXJ1538.9-3116	15 38 55.2	-31 16 31	PTTS		VB[4]
RXJ1539.0-2956	15 39 01.8	-29 56 30	????		
RXJ1539.4-2958	15 39 25.0	-29 58 44	PTTS		
RXJ1539.4-3446A	15 39 25.2	-34 46 49	????	HIP 76675	
RXJ1539.4-3446B	15 39 27.9	-34 46 16	CTTS		
RXJ1539.4-3446C	15 39 27.9	-34 46 16	CTTS		
RXJ1539.5-2953	15 39 33.8	-29 53 30	PTTS		VB[4]
RXJ1540.2-3018	15 40 12.2	-30 18 30	PTTS		
RXJ1540.7-3121A	15 40 45.6	-31 21 12	PTTS		
RXJ1540.7-3121B	15 40 45.6	-31 21 12	PTTS		
RXJ1540.9-3024	15 40 55.4	-30 24 18	PTTS		
RXJ1541.9-3019	15 41 56.2	-30 19 00	PTTS		
RXJ1543.4-2925	15 43 29.2	-29 25 34	????		SB[7]
RXJ1543.8-3306	15 43 33.0	-33 04 30	????		VB[4,6]
RXJ1544.0-3311	15 44 03.6	-33 11 11	????		VB[3,4]
RXJ1544.2-3117	15 44 16.6	-31 17 12	????		
RXJ1545.2-3417	15 45 12.0	-34 17 30	CTTS	HIP 77157	VB[4]
RXJ1545.5-3249	15 45 32.1	-32 49 36	????		
RXJ1545.6-3208	15 45 35.3	-32 08 49	????		
RXJ1545.8-3020	15 45 47.6	-30 20 52	PTTS	HIP 77199	
RXJ1546.0-2920	15 46 05.5	-29 20 40	PTTS		
RXJ1546.1-2804	15 46 10.8	-28 04 22	????		VB[4]
RXJ1546.7-3210	15 46 47.0	-32 10 06	PTTS		
RXJ1548.0-2908	15 48 02.9	-29 08 36	????		
RXJ1548.9-3045	15 48 57.1	-30 45 00	PTTS		
RXJ1549.0-3102	15 49 02.7	-31 02 52	WTTS		
RXJ1549.3-2600	15 49 21.0	-26 00 05	WTTS		VB[4]
RXJ1550.0-2312	15 50 05.0	-23 11 53	????		
RXJ1550.9-2534	15 50 56.4	-25 34 18	????		SB[7]
RXJ1551.1-2402	15 51 06.6	-24 02 19	PTTS		
RXJ1551.4-3131	15 51 26.8	-31 30 59	PTTS		VB[3,4]
RXJ1551.9-2621	15 51 54.4	-26 22 04	????		

TABLE 7
TARGET LIST (CONTINUED)

Target name	α (2000)	δ (2000)	TTS class	Alias	remark
RXJ1552.5-3224A	15 52 30.0	-32 24 12	PTTS		VB[3,4]
RXJ1552.5-2633	15 52 31.3	-26 33 51	PTTS		
RXJ1554.0-2920	15 54 03.6	-29 20 15	PTTS		VB[3,4]
RXJ1554.9-2347	15 54 59.9	-23 47 18	????	NTTS155203-2338, ScoPMS 005	VB[3,4]
RXJ1555.1-2521	15 55 06.2	-25 21 09	PTTS		VB[4]
NTTS155219-2314	15 55 17.1	-23 22 16	PTTS	ScoPMS 008b	
NTTS155220-2313	15 55 18.6	-23 22 06	????	ScoPMS 008a	VB[4]
RXJ1555.4-3338	15 55 26.2	-33 38 23	PTTS		
RXJ1555.6-3159	15 55 37.0	-31 59 58	PTTS		VB[3]
RXJ1555.8-2512	15 55 48.8	-25 12 23	????		
NTTS155331-2340	15 56 29.4	-23 48 19	PTTS	ScoPMS 013	VB[4]
NTTS155357-2321	15 56 54.9	-23 29 46	????	ScoPMS 014	
RXJ1557.3-2529	15 57 16.7	-25 29 18	PTTS		VB[4]
NTTS155421-2330	15 57 20.0	-23 38 49	PTTS	ScoPMS 015	
NTTS155427-2346	15 57 25.8	-23 54 22	WTTS	ScoPMS 016	VB[4]
NTTS155436-2313	15 57 34.4	-23 21 11	WTTS	ScoPMS 017	
RXJ1557.8-2305	15 57 50.0	-23 05 09	PTTS		
RXJ1558.1-2405B	15 58 07.4	-24 05 54	????		VB[4]
RXJ1558.1-2405A	15 58 08.2	-24 05 52	PTTS		
RXJ1558.2-2328	15 58 12.7	-23 28 36	????		
RXJ1558.8-2512	15 58 53.6	-25 12 32	????		
RXJ1559.2-2606	15 59 14.5	-26 06 18	????		VB[3,4]
RXJ1559.6-3255	15 59 36.7	-32 55 36	????		
RXJ1559.8-2556	15 59 50.1	-25 55 58	PTTS		VT[6]
NTTS155703-2212	16 00 00.0	-22 20 37	PTTS	ScoPMS 019	
RXJ1600.0-2509	16 00 00.8	-25 09 42	????		
RXJ1600.2-2417	16 00 13.3	-24 18 10	PTTS		
RXJ1600.5-2027	16 00 31.4	-20 27 05	PTTS		VB[4]
RXJ1600.6-2159	16 00 40.6	-22 00 32	????		
RXJ1600.7-2127	16 00 42.8	-21 27 38	PTTS		
RXJ1600.7-2343	16 00 44.6	-23 43 12	????		VB[4]
NTTS155808-2219	16 01 05.2	-22 27 31	WTTS	ScoPMS 020	SB2[1], VB[4]
RXJ1601.1-2113	16 01 08.1	-21 13 19	PTTS		
RXJ1601.3-2652	16 01 18.4	-26 52 20	????	HIP 78483	VB[4]
RXJ1601.4-2240	16 01 25.7	-22 40 40	WTTS	NTTS155828-2232, ScoPMS 021	
RXJ1601.7-2049	16 01 46.5	-20 49 46	PTTS		VB[4]
RXJ1601.8-2445	16 01 51.5	-24 45 25	PTTS		VB[4]
RXJ1601.9-2008	16 01 58.2	-20 08 12	????		
RXJ1602.0-2221	16 02 00.4	-22 21 24	PTTS		
NTTS155910-2247	16 02 08.5	-22 54 57	PTTS	ScoPMS 022	
RXJ1602.1-2241	16 02 10.4	-22 41 28	????	NTTS155913-2233, ScoPMS 023	SB2[1,7], VB[2,4]
RXJ1602.8-2401B	16 02 51.3	-24 01 57	WTTS		
RXJ1602.8-2401A	16 02 52.4	-24 02 22	????		
RXJ1602.9-2022	16 02 54.0	-20 22 48	PTTS		VB[4]
RXJ1603.6-2245	16 03 35.5	-22 45 56	????		
RXJ1603.9-2031B	16 03 55.0	-20 31 39	PTTS		VB[4]
RXJ1603.9-2031A	16 03 57.7	-20 31 06	CTTS		
RXJ1604.3-2130B	16 04 20.9	-21 30 42	PTTS		VB[4,6]
RXJ1604.3-2130A	16 04 21.7	-21 30 29	CTTS		
RXJ1604.7-1930	16 04 47.8	-19 30 23	????	NTTS160153-1922, ScoPMS 027	
NTTS160233-1931	16 05 27.3	-19 38 46	WTTS	ScoPMS 028	
RXJ1605.6-2152	16 05 38.9	-21 52 32	PTTS		
RXJ1605.7-2004	16 05 42.7	-20 04 15	WTTS	NTTS160248-1956, ScoPMS 029	VB[4]
RXJ1606.2-2036	16 06 12.6	-20 36 47	WTTS		
RXJ1606.3-1928	16 06 22.0	-19 28 44	CTTS	NTTS160328-1921, ScoPMS 031	VB[4]
RXJ1606.6-2108	16 06 37.4	-21 08 41	PTTS		VB[4]

TABLE 7
TARGET LIST (CONTINUED)

Target name	α (2000)	δ (2000)	TTS class	Alias	remark
NTTS160345-1953	16 06 39.9	-20 01 28	WTTS	ScoPMS 032	
RXJ1607.0-2043	16 07 03.1	-20 43 20	WTTS		
RXJ1607.0-1911	16 07 03.9	-19 11 33	PTTS		VB[4]
RXJ1607.0-2036	16 07 03.6	-20 36 26	WTTS		
NTTS160728-1856	16 10 21.7	-19 04 06	PTTS	ScoPMS 042b	
NTTS160735-1857	16 10 28.6	-19 04 46	WTTS	ScoPMS 042a	VB[4]
NTTS160814-1857	16 11 08.9	-19 04 46	WTTS	ScoPMS 044	SB[1]
NTTS160827-1813	16 11 20.6	-18 20 54	PTTS	ScoPMS 045	
NTTS160836-1843	16 11 29.8	-18 50 53	????	ScoPMS 046	
NTTS160905-1859	16 11 59.2	-19 06 52	WTTS	ScoPMS 048	SB[1]
NTTS160927-1901	16 12 20.9	-19 09 04	WTTS	ScoPMS 051	
NTTS160946-1851	16 12 40.5	-18 59 27	WTTS	ScoPMS 052	VB[4]
NTTS161431-2256	16 17 31.4	-23 03 34	????	ScoPMS 060	

NOTE.— SB: Spectroscopic Binary, VB: Visual Binary, VT: Visual Triple, EB: Eclipsing Binary

REFERENCES.—[1] Mathieu, Walter, & Myers 1989, Walter et al. 1994, [2] Ghez et al. 1993, [3] Brandner et al. 1996, [4] Köhler 1997, Köhler et al. 2000, [5] Neuhäuser & Brandner 1998, [6] Brandner et al., in prep, [7] this paper

TABLE 8
REVISED MASSES AND AGES FOR STARS WITH HIPPARCOS PARALLAXES.

Name	Parallax [mas]	Distance [pc]	$mass_{145pc}$ [$M_\odot$]	$mass_{HIP}$ [$M_\odot$]	$\log(age_{145pc})$ [yr]	$\log(age_{HIP})$ [yr]
RXJ1528.7-3117	11.5±2.6[1]	87.0	1.73	**1.23**	6.74	**7.10**
RXJ1529.4-2850A	11.2±1.5[1]	89.7	1.82	**1.27**	6.67	**7.10**
RXJ1530.4-3218	10.9±3.3[1]	91.7	1.66	**1.24**	6.81	**7.11**
RXJ1535.2-2828	12.6±1.1	79.6	1.79	**1.24**	6.76	**7.21**
RXJ1539.4-3446A	13.6±1.2	73.5	1.45	**1.10**	7.02	**7.56, ZAMS?**[2]
RXJ1545.2-3417	6.3±2.1	159.0	1.80	**1.91**	6.60	**6.52**
RXJ1545.8-3020	24.4±1.4[1]	40.9	2.00	**0.94**	5.52	**7.35**
RXJ1601.3-2652	6.7±1.6	150.4	1.28	**1.38**	7.15	**7.09**
Average:			1.69±0.23	**1.29±0.28**	6.66±0.49	**7.13±0.30**

NOTE.—[1]see also Neuhäuser & Brandner 1998; [2]possibly a Zero-Age-Main-Sequence (ZAMS) star